Accepted Manuscript

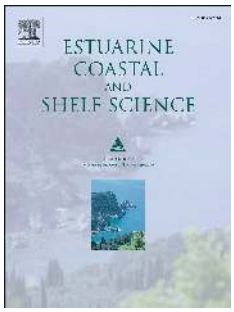

Stem breakage of salt marsh vegetation under wave forcing: A field and model study

Vincent Vuik, Hannah Y. Suh Heo, Zhenchang Zhu, Bas W. Borsje, Sebastiaan N. Jonkman

PII: S0272-7714(17)30391-8

DOI: 10.1016/j.ecss.2017.09.028

Reference: YECSS 5630

To appear in: *Estuarine, Coastal and Shelf Science*

Received Date: 10 April 2017

Revised Date: 15 September 2017

Accepted Date: 26 September 2017

Please cite this article as: Vuik, V., Suh Heo, H.Y., Zhu, Z., Borsje, B.W., Jonkman, S.N., Stem breakage of salt marsh vegetation under wave forcing: A field and model study, *Estuarine, Coastal and Shelf Science* (2017), doi: 10.1016/j.ecss.2017.09.028.

Stem breakage of salt marsh vegetation under wave forcing: a field and model study

Vincent Vuik[1,2] Hannah Y. Suh Heo[1] Zhenchang Zhu[3]
Bas W. Borsje[4,5] Sebastiaan N. Jonkman[1]

[1]Delft University of Technology, Civil Engineering & Geosciences, P.O. Box 5048, 2600 GA Delft, The Netherlands
[2]HKV Consultants, P.O. Box 2120, 8203 AC Lelystad, The Netherlands
[3]Netherlands Institute for Sea Research (NIOZ), Korringaweg 7, 4401 NT Yerseke, The Netherlands
[4]University of Twente, Water Engineering & Management, P.O. Box 217, 7500 AE Enschede, The Netherlands
[5]Board Young Waddenacademie, Ruiterskwartier 121a, 8911 BS, Leeuwarden, The Netherlands

Abstract

One of the services provided by coastal ecosystems is wave attenuation by vegetation, and subsequent reduction of wave loads on flood defense structures. Therefore, stability of vegetation under wave forcing is an important factor to consider. This paper presents a model which determines the wave load that plant stems can withstand before they break or fold. This occurs when wave-induced bending stresses exceed the flexural strength of stems. Flexural strength was determined by means of three-point-bending tests, which were carried out for two common salt marsh species: *Spartina anglica* (common cord-grass) and *Scirpus maritimus* (sea club-rush), at different stages in the seasonal cycle. Plant stability is expressed in terms of a critical orbital velocity, which combines factors that contribute to stability: high flexural strength, large stem diameter, low vegetation height, high flexibility and a low drag coefficient. In order to include stem breakage in the computation of wave attenuation by vegetation, the stem breakage model was implemented in a wave energy balance. A model parameter was calibrated so that the predicted stem breakage corresponded with the wave-induced loss of biomass that occurred in the field. The stability of *Spartina* is significantly higher than that of *Scirpus*, because of its higher strength, shorter stems, and greater flexibility. The model is validated by applying wave flume tests of *Elymus athericus* (sea couch), which produced reasonable results with regards to the threshold of folding and overall stem breakage percentage, despite the high flexibility of this species. Application of the stem breakage model will lead to a more realistic assessment of the role of vegetation for coastal protection.

Keywords: salt marsh; vegetation; wave attenuation; stem breakage model; three-point-bending test; coastal protection

1 Introduction

Many countries have to cope with the effects of sea level rise and land subsidence along their densely populated coastlines, which leads to an increase in flood hazards. Coastal ecosystems, such as salt marshes, mangrove forests and reed swamps, provide a wide range of ecosystem services, including wave attenuation, shoreline stabilization and sediment trapping (Barbier et al., 2011; Duarte et al., 2013). These ecosystems act as vegetated foreshores at places where they are situated in front of engineered flood defense structures. Foreshores potentially reduce the impact of surges and waves on the structures (Arkema et al., 2013), since waves reduce in height and intensity due to both wave breaking in shallow water and wave attenuation by vegetation.

Many studies quantify wave attenuation by vegetation, based on field and laboratory measurements (see Vuik et al. (2016) for an overview) or numerical models (Suzuki et al., 2012; Tang et al., 2015). Its magnitude depends on hydrodynamic parameters, such as wave height (Anderson and McKee Smith, 2014), wave period (Jadhav et al., 2013) and water depth (Paquier et al., 2016), and on vegetation characteristics, such as stem height, diameter and density (Marsooli and Wu, 2014) and flexibility (Luhar and Nepf, 2016; Paul et al., 2016).

The wave attenuation capacity of vegetation varies throughout the year, because of seasonal variations in above-ground biomass (Drake, 1976). One of the factors that drive the variation in biomass, is wave-induced stem breakage of the vegetation. This breakage process varies in time due to seasonal differences in storm frequency and intensity, and a seasonal cycle in the mechanical strength of the stems (Liffen et al., 2013).

Depending on the geographical location, extreme conditions may occur in different seasons. For instance, the Gulf coast of the USA is mainly affected by hurricanes from August to October, whereas coasts around the North Sea in Europe are primarily affected by storm surges between November and February. Vegetation also has its seasonal cycle: above-ground structures of mangroves and tropical seagrasses are present all year-round, while salt marsh plants in temperate climates lose much of their above-ground biomass during the winter (Gallagher, 1983; Koch et al., 2009; Bouma et al., 2014). The coinciding seasonal variations in storm intensity and vegetation characteristics determine to what extent vegetation may contribute to wave load reduction on flood defenses.

Puijalon et al. (2011) describe two strategies of plants to deal with drag forces due to wind or water movement: an avoidance strategy, where plants minimize the encountered forces, or a tolerance strategy, where plants maximize their resistance to breakage. Flexible plant species show an avoidance strategy, minimizing the risk of folding and breakage through reconfiguration. Stiff plants are more efficient in attenuating waves, as they maximize their resistance to stress (Paul et al., 2016), but may break at a certain threshold, which leads to a decline in wave attenuation capacity. A stem will fold or break when the wave-induced bending stress exceeds the stem's strength (Heuner et al., 2015; Silinski et al., 2015). Folding is an irreversible deformation, which leads to a lower effective plant height for wave attenuation. Folded stems may eventually break, and the biomass on the salt marsh decreases. The broken vegetation is frequently found in the form of accumulated debris on dike slopes after storms (Grüne, 2005). Remainders of broken vegetation will only contribute to wave energy reduction by enhancing the roughness of the bottom compared to non-vegetated surfaces.

Vegetation causes wave attenuation due to the force exerted by the plants on the moving water. Following Newton's third law, the water simultaneously exerts a force equal in magnitude and opposite in direction on the plants. The flexibility of the plants determines how plant motion and wave motion interact, and determines the magnitude of the drag forces (Bouma et al., 2005; Dijkstra and Uittenbogaard, 2010; Mullarney and Henderson, 2010). Luhar and Nepf (2016) propose two dimensionless numbers to describe the motion of flexible vegetation under wave forcing: (1) the Cauchy number C_a, which represents the ratio of the hydrodynamic forcing to the restoring force due to stiffness, and (2) the ratio of the stem height to the wave orbital excursion, L. Plants will stand upright, and act as stiff cylinders, for $C_a < 1$. For $C_a > 1$, the vegetation will start to bend and move in the oscillatory flow. The ratio L determines the characteristics of the plant motion, with swaying motion for $L > 1$, and flattening of the vegetation for $L < 1$. Flattening of the vegetation leads to low flow resistance for a part of the wave cycle.

Several studies show that a significant loss of above-ground biomass can occur during storms (Seymour et al., 1989; Howes et al., 2010). Stem breakage was also observed in large-scale flume experiments on wave attenuation by vegetation (Möller et al., 2014). Recently, Rupprecht et al. (2017) determined the loss of biomass during these experiments, and related it to the measured wave orbital velocities in the canopy. They studied the impact of wave heights in the range of 0.1-0.9 m on two different salt marsh grasses: low-growing and highly flexible *Puccinellia maritima* and more rigid and tall *Elymus athericus*. *Puccinellia* survived even the highest wave

forcing without substantial physical damage. This indicates that this species shows an avoidance strategy (Bouma et al., 2010).

The role of vegetation for coastal protection is increasingly accepted in flood risk management (Temmerman et al., 2013). However, actual implementation of vegetation into coastal protection schemes is often hampered by a lack of knowledge on how vegetation behaves under extreme storm conditions (Anderson et al., 2011; Vuik et al., 2016). The quantification of wave-induced stem breakage by Rupprecht et al. (2017) is a major step forward in the assessment of the resilience of salt marsh vegetation to storm surge conditions. However, the quantification is purely empirical, and application to other plant species or hydrodynamic conditions is difficult. Further, large-scale flume experiments as in Möller et al. (2014) are expensive and labor-intensive. As a result, we aim to develop a method that predicts the relation between orbital velocity and biomass loss, as a function of plant characteristics such as plant morphology (stem height and diameter) and stem strength. We only consider biomass loss due to stem breakage. Uprooting may be another relevant mechanism, but we did not observe this phenomenon in the field. However, it may be relevant for different species, soil conditions or wave conditions (Liffen et al., 2013).

This paper presents a model that predicts the wave load that plant stems can withstand before they break or fold. The model compares bending stresses, induced by the orbital motion under waves, with the flexural strength of stems. Plant stability is expressed in terms of a critical orbital velocity, which combines plant morphology (stem height and diameter) and stem strength. The flexural strength is determined based on three-point bending tests, which were conducted in the laboratory for two common salt marsh species: common cord-grass (*Spartina anglica*) and sea club-rush (*Scirpus maritimus*). Stems were collected from salt marshes at different stages in the seasonal cycle of the plants, to capture the temporal variation in strength. The model is calibrated by relating the loss of biomass that took place on two salt marshes in the Netherlands to the wave conditions that were measured at these marshes over 19 months. Finally, the model is validated by applying flume tests of *Elymus athericus* (sea couch) presented in Rupprecht et al. (2017).

2 Methods and materials

2.1 Field sites and plant species

Two salt marshes in the Western Scheldt of the Netherlands were selected as field sites for the wave and vegetation measurements (Fig. 1). The first location is Hellegat, where *Spartina anglica* (common cord-grass) is the dominant plant species, and the second is Bath where *Scirpus maritimus* (sea club-rush) is prevalent. The bathymetry of both sites was measured using RTK-DGPS (Leica Viva GS12), see Fig. 1.

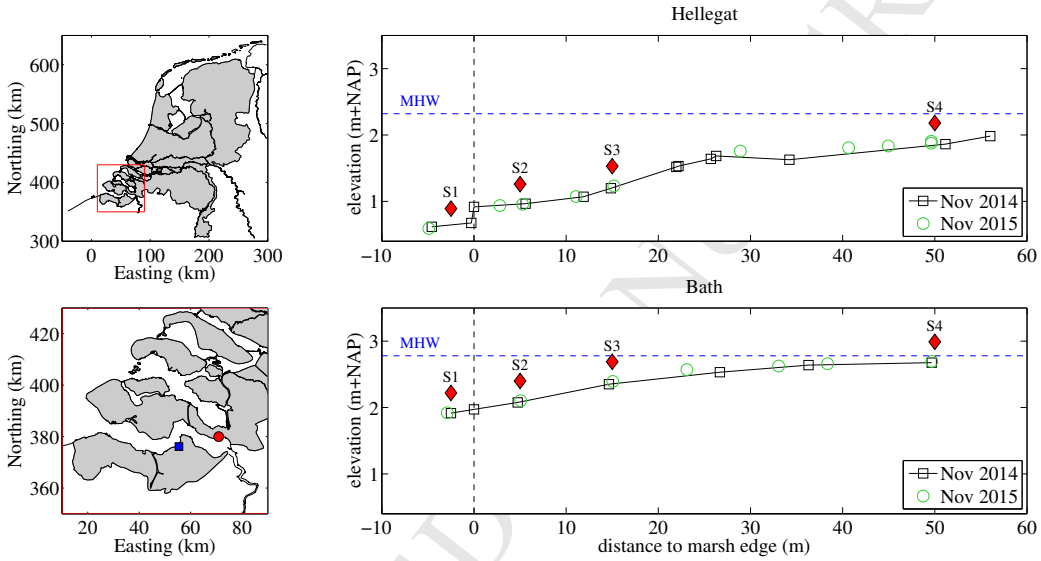

Figure 1: Location of the salt marshes Hellegat (blue square) and Bath (red circle) in the Western Scheldt estuary (lower left) in the Netherlands (upper left), and the bathymetry at the measurement transects at Hellegat (upper right) and Bath (lower right) for November 2014 (black) and November 2015 (green). The position of the 4 wave gauges S1-S4 is indicated by red diamonds. The vertical dashed line is positioned at the marsh edge, the horizontal dashed line at Mean High Water.

Hellegat is located at the southern shore of the Western Scheldt, and is exposed to waves from directions between west and north. The marsh edge has an elevation of approximately NAP+1.0 m, where NAP is the Dutch reference level, close to mean sea level. A small cliff of 25 cm height is present at the marsh edge. Landward of the cliff, the bottom is sloping over a distance of approximately 50 m to the higher parts of the marsh, at NAP+2.0 m. The tide

in the Western Scheldt leads to a local high water level of NAP+1.6 m at neap tide and up to NAP+2.9 m at spring tide. The highest water levels in the Western Scheldt occur during north-westerly storms in the North Sea region. That implies that Hellegat is regularly exposed to high waves and water levels at the same time. Bath is situated more upstream in the Western Scheldt, along the dike at the northern shore of the estuary, close to the bend towards Antwerp. High water levels in the tidal cycle are higher here, between NAP+1.9 m (neap tide) and NAP+3.4 m (spring tide). This has led to a high salt marsh elevation, sloping from NAP+2.0 m at the marsh edge to NAP+2.7 m at a distance of 50 m from the edge. No cliff is present at the marsh edge here. This marsh is more sheltered compared to Hellegat during north-westerly storms, due to its orientation towards the south-west.

While the salt marsh at Bath is dominated by *Scirpus*, there are also some patches with *Spartina* present (Fig. 2). In September, both species are standing up straight to a large extent. The difference in stem density is clearly visible. Especially for *Scirpus*, the start of the decay of the plants in autumn is already visible. In the photo from January, almost all *Scirpus* has disappeared, and only broken stems are remaining. In contrast, in the *Spartina* zone, there is still a lot of biomass present, with a mix of standing and folded stems.

2.2 Wave measurements

Wave attenuation was measured for *Spartina* at Hellegat, and for *Scirpus* at Bath. At both sites, 4 wave gauges (Ocean Sensor Systems, Inc., USA) were deployed over a total distance of 50 m, measured from the marsh edge. One wave gauge (indicated by S1) was placed at 2.5 m in front of the marsh edge. The other gauges were placed at 5 (S2), 15 (S3) and 50 m (S4) in the vegetation. The pressure sensors on the gauges were mounted 10 cm from the bottom. The pressure was recorded with a frequency of 5 Hz over a period of 7 min, every 15 min. Wave energy spectra were determined, using Fast Fourier Transformation, taking into account the attenuation of the pressure signal with depth. A more detailed description of the measurements and processing of the data can be found in Vuik et al. (2016), who made use of data that was collected between November 2014 and January 2015. The present study analyzes wave data for a considerably longer period of 19 months, from November 2014 to May 2016, for which all wave gauges were continuously operational. This enables the analysis of seasonal variations in wave attenuation.

In order to analyze the seasonal differences in wave attenuation by vegetation, the mean wave height reduction between gauges S1 and S4 is computed for each month. However, the wave

(a) *Spartina* (left) and *Scirpus* (right), 16 September 2015

(b) *Spartina* (left) and *Scirpus* (right), 19 January 2017

Figure 2: Photos of *Spartina* and *Scirpus* next to each other, in late summer (top) and in winter (bottom). Photos taken by Zhenchang Zhu at Bath.

height reduction does not only depend on vegetation characteristics, but also on the prevalent hydrodynamic conditions such as water depth, wave height and wave period (Tschirky et al., 2001). When simply considering the mean wave height reduction per month, the numbers are strongly influenced by the fact that storms with large water depths and wave heights occur far more frequently in winter than in summer. To eliminate such seasonal differences in storm intensity and frequency, variations in wave attenuation are analyzed for different sea states. Sea states consist of a combination of a wave height range (e.g. 0.1-0.2 m) and a water depth range

(e.g. 1.50-1.75 m) at the marsh edge. For all measurements in this range in each month, the average wave height reduction over 50 m transect length $(H_{m0,0} - H_{m0,50})/H_{m0,0}$ is computed. Sea states are selected, based on the criteria of (1) sufficient occurrence in all months and (2) inundation of the full transect (Table 1), where the water depth at 50 m in the marsh is 1.28 m and 0.77 m lower than on the mudflat at Hellegat and Bath, respectively.

Table 1: Selected sea states, for which the monthly average wave height reduction over 50 m salt marsh was determined at Hellegat (H) and Bath (B).

h (m)	H_{m0} (m)		
at mudflat	0.0-0.1	0.1-0.2	0.2-0.3
1.00-1.25	B	B	
1.25-1.50	B	B	
1.50-1.75	H	H	H
1.75-2.00	H	H	H
2.00-2.25	H	H	H

2.3 Quantifying vegetation strength

At the two salt marshes, Hellegat and Bath, approximately 20-30 stems of each species were sampled four times in the seasonal cycle: 3 Dec. 2014, 7 Apr. 2015, 11 Sep. 2015 and 4 Nov. 2015 (*Spartina*), and 5 Dec. 2014, 1 Apr. 2015, 4 Sep. 2015 and 4 Nov. 2015 (*Scirpus*). For every stem, the stem diameter at approximately 5 cm from the bottom and the entire stem length were measured and then taken to the lab for further testing. As one of the important steps to quantify stem strength, three-point bending tests of the stems were performed at the Royal Netherlands Institute for Sea Research (NIOZ). Conventionally, the three-point bending test is used to find the stress-strain relationship of a material in structural mechanics (or ecology), which in particular, focuses on the initial deflection behavior with a small amount of applied force (Usherwood et al., 1997; Dijkstra and Uittenbogaard, 2010; Miler et al., 2012; Paul et al., 2014; Rupprecht et al., 2015). However, this research considers the extreme situation when the stress-strain relation of the material (stem) is no longer linear and reaches its maximum flexural stress (Fig. 4). The stem is considered to break or fold when it reaches this maximum bending stress which is defined as the individual stem's flexural strength. This strength is determined for the bottom 5-10 cm of the stems (5cm for *Spartina* and 10 cm for *Scirpus*), as this is the location

where the stems of both species normally break (see Fig. 2 and the information in Section 2.7). The stem density was measured by counting the number of standing stems in 10 sample areas of 25*25 cm at both Hellegat and Bath: 5 sample areas high in the marsh, and 5 close to the marsh edge.

For the hollow stemmed *Spartina*, the outer and inner diameter of each stem was measured with an electronic caliper (precision ± 0.5 mm), and the three-point bending test device's span length was fixed to 40 mm, resulting in a stem-diameter-to-span-length ratio between 1:10 and 1:14. *Scirpus* is not hollow, and the length of the three sides of the triangular cross-section was measured with the electronic caliper. In order to minimize the effect of shear stress, a maximum stem-diameter-to-span-length ratio of 1:15 was chosen for *Scirpus*. The three-point bending test's span length was adjusted to 15 times the mean side length. The bending tests were performed with an Instron EMSYSL7049 flexure test machine (precision ± 0.5%) using a 10 kN load cell (Instron Corporation, Canton, MA, USA) (Fig. 3). The stem test section was placed centrally onto two supporting pins, and a third loading pin was lowered from above at a rate of 10 mm/min. The vertical deflection of the stem and the corresponding force were recorded.

Figure 3: The Instron three-point bending test device

The flexural strength of the stem, expressed in terms of bending stress, is calculated by

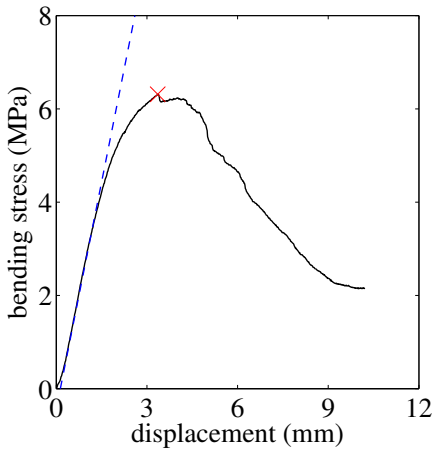

Figure 4: Example of a stress-strain relation (solid black line) from results of a three-point bending test. Young's modulus (E) and flexural rigidity (EI) can be calculated from the slope of the initial linear part (blue dashed line). The plant breaks or folds when the line reaches its maximum bending stress, indicated with a red marker. This stress-strain relation is representative for many vegetation species including *Spartina anglica* and *Scirpus maritimus*.

standard formulas in structural mechanics. The maximum tolerable bending stress σ_{max} (Nm^{-2}) is calculated as

$$\sigma_{max} = M_{max} y / I, \tag{1}$$

where M_{max} is the maximum moment (Nm); y is the cross-sectional distance from the center of the cross-section to the convex surface (m), and I is the area moment of inertia (m^4). The maximum moment, $M_{max} = (1/4) F_{max} L_{span}$, is a function of the maximum force F_{max} (N) and the testing device's span length L_{span} (m). The two species studied in this research, *Spartina* and *Scirpus*, have different cross-sectional stem geometries. As a result, the cross-sectional distance and area moment of inertia are quantified differently (Fig. 5). Here, the stem diameter is indicated as b_v, and for vegetation with a hollow stem (*Spartina*), the inner diameter is represented as $b_{v,in}$.

Formulas for M_{max}, y and I (Fig. 5) are substituted in Eq. (1). The resulting flexural strength of the hollow, circular stems of *Spartina* is then expressed as

$$\sigma_{max,cir} = \frac{8 F_{max} L_{span} b_v}{\pi \left({b_v}^4 - {b_{v,in}}^4 \right)}, \tag{2}$$

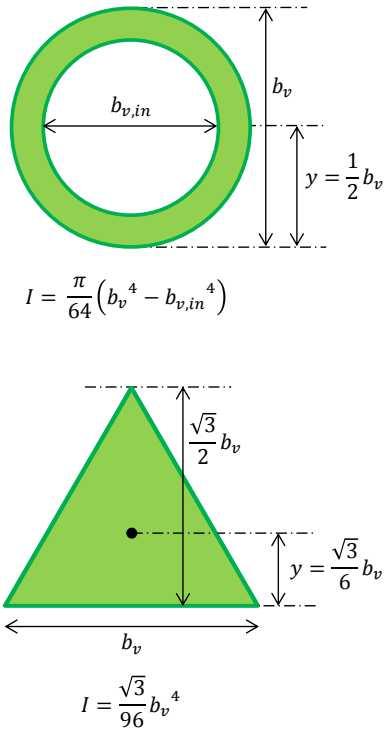

Figure 5: The stem cross-section of *Spartina anglica* and *Scirpus maritimus*. *Spartina anglica* has a hollow circular stem (top), whereas *Scirpus maritimus* has a solid triangular stem, which is assumed to be equilateral (bottom). Formulas for calculating y (cross-sectional distance from center to convex surface) and I (area moment of inertia) are based on the stem geometry.

and for the triangular stems of *Scirpus* as

$$\sigma_{max,tri} = \frac{4 F_{max} L_{span}}{{b_v}^3}. \tag{3}$$

Mean values and standard deviations for the different parameters are determined for the sample locations close to the marsh edge and higher in the marsh separately. After that, the average mean value and average standard deviation are computed, and presented in this paper. This means that the presented standard deviations reflect the average in-sample variation, rather than the inter-sample variation in vegetation properties.

2.4 Quantifying wave-induced bending stress

The amount of wave load acting on the stem is also quantified in terms of bending stress, in order to be comparable to the flexural strength. In Fig. 6 (left), vegetation is first schematized as a standing, cantilevering beam attached to a fixed bottom with a uniform horizontal load acting on the entire length of the stem. In such case, the critical bending stress acting at the bottom of the stem can be expressed as

$$\sigma_{wave} = \frac{q_D(\alpha h)^2 y}{2I}, \tag{4}$$

from standard structural mechanics (Gere and Goodno, 2013). Here, q_D is the drag force per unit plant height (N/m) and $\alpha = \min(h_v/h, 1)$ is the stem height h_v relative to the water depth h, maximized to 1 for emergent conditions. The drag force q_D is assumed to be uniform along the plant height which is in line with shallow water wave conditions.

In the wave-induced stress equation (σ_{wave}), stem height h_v and diameter b_v are known from field measurements, and the area moment of inertia I can be calculated based on the stem geometry and diameter (Fig. 5). The uniform wave load q_D is calculated by modifying the Morison-type equation F_x, previously used by Dalrymple et al. (1984) and Kobayashi et al. (1993). When dividing the Morison-type equation F_x by the stem density N_v (stems/m^2), this yields the uniform wave load q_D, which is expressed in terms of force per unit area per unit height (Nm^{-2}m^{-1}) as

$$q_D = \frac{F_x}{N_v} = \frac{1}{2}\rho C_D b_v u|u|, \tag{5}$$

where C_D is the bulk drag coefficient (-), ρ the density of water (kg/m^3), and u is the horizontal orbital velocity of waves (m/s). The uniform horizontal wave load q_D yields the force per unit length of stem. Under shallow water conditions, the orbital velocity is expressed in terms of wave height H (m), water depth h (m) and gravitational acceleration g (m/s^2) as $u = 0.5H\sqrt{g/h}$. Substituting the expressions for q_D and u into Eq. (4), the wave-induced bending stress at the bottom of the stem can be described with vegetation and wave parameters for circular and triangular stems. There is no information available to identify which individual wave from the random wave field leads to stem breakage. However, it makes sense that it should represent the forces exerted by the highest fraction of the waves. Therefore, we assume that the mean of

the highest one-tenth of waves breaks the stems ($H = H_{1/10}$). This measure is related to the significant wave height H_{m0} (=mean of the highest one-third of waves) via $H_{1/10} = 1.27H_{m0}$, assuming a Rayleigh distribution. The possible bias caused by this assumption will influence the results of the model calibration.

A correction factor is needed for the wave-induced load to take into account uncertainties involved in the selection of $H_{1/10}$, and in physical processes that are not explicitly included in the equations, such as fatigue and reduction of orbital velocities in the canopy. The equations for wave load are multiplied with an adjustable correction factor A_c, to account for such processes. The correction factors are calibrated for both species based on the amount of breakage in response to wave action in the field. Stem leaning and bending will be implemented as a separate factor, which will be discussed next.

Prior to calibrating the correction factor, the known but neglected process of stem leaning is assessed. So far, for the quantification of stem strength and wave-induced stress, the stem was assumed to be a relatively stiff beam standing up straight (90° from the sea bed). However, in reality the stems are quite flexible. This flexibility not only serves to reduce the amount of wave forcing but also prevents the weakest point along the stem (susceptible to breaking) from being directly exposed to strong wave forces.

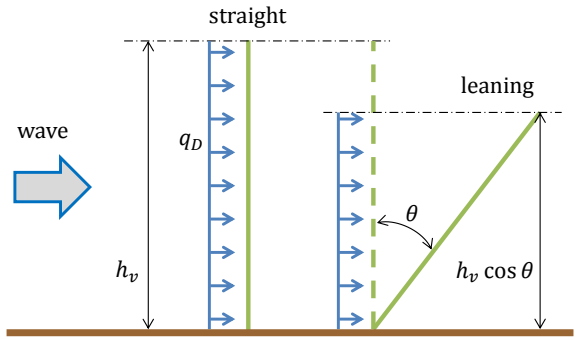

Figure 6: The stem standing up straight (left) represents the preliminary consideration where the entire height of the stem (h_v) experiences the uniform horizontal wave loading. The leaning stem (right) represents the more realistic case, with a leaning angle θ which experiences a smaller horizontal wave load along the height of $h_v \cos\theta$.

The stem leaning angle varies widely depending on the combined direction and strength of

the wave. However, in this research one representative leaning angle is chosen for each species based on field observations and its respective flexural rigidity (EI). From observations of Silinski et al. (2015), adult *Scirpus* has a maximum observed leaning angle of $\theta = 15°$ for short-period (2 s) waves and $\theta = 40°$ for long-period (10 s) waves. Wave peak periods at Bath are in the order of 3-4 s during storms, which is in between the two extremes of Silinski et al. Therefore, a leaning angle of 30° will be used in this research for *Scirpus*. Bouma et al. (2005) gives a maximum leaning angle of $\theta = 51°$ for *Spartina*, which is a larger angle than that of *Scirpus*. This is in line with the smaller flexural rigidity (EI) of *Spartina* (1000-4000 Nmm^2 in Rupprecht et al. (2015), 2100 ± 1000 Nmm^2 in the current study, Table 3), compared to *Scirpus* (40,000-50,000 Nmm^2 in Silinski et al. (2015), $52{,}000 \pm 35{,}000$ Nmm^2 in the current study, Table 4) With the maximum leaning angle (θ) for each species, the wave load is corrected by multiplying it with $\cos^2\theta$, as the submerged vegetation height ($h_v = \alpha h$) is squared as can be seen in Eq. (4).

The resulting wave-induced stress in shallow water wave conditions for the hollow, circular stems of *Spartina* is then expressed as

$$\sigma_{wave,cir} = 2A_c \rho g C_D \left(\frac{b_v^2 (\alpha h)^2 \cos^2\theta}{\pi \left(b_v^4 - b_{v,in}^4 \right)} \right) \left(\frac{H_{1/10}^2}{h} \right), \tag{6}$$

and in the solid triangular stems of *Scirpus* as

$$\sigma_{wave,tri} = A_c \rho g C_D \left(\frac{(\alpha h)^2 \cos^2\theta}{b_v^2} \right) \left(\frac{H_{1/10}^2}{h} \right). \tag{7}$$

2.5 Definition of vegetation stability

Stem folding or breaking is identified as the point when the wave-induced bending stress exceeds the stem's flexural strength. The stability of vegetation under wave forcing can be investigated by comparing flexural strength σ_{max} (Eq. (2) or Eq. (3)) with the corresponding wave-induced stress σ_{wave} (Eq. (6) or Eq. (7)) for *Spartina* and *Scirpus*, respectively.

By combining the equations (4) and (5), and including the leaning factor $\cos^2\theta$ and correction factor A_c, the critical orbital velocity for the circular stems of *Spartina* can be expressed as

$$u_{crit,cir} = \sqrt{\frac{\sigma_{max} \pi \left(b_v^4 - b_{v,in}^4 \right)}{8 A_c \rho C_D b_v^2 (\alpha h)^2 cos^2\theta}}, \tag{8}$$

and for the triangular stems of *Scirpus* as

$$u_{crit,tri} = \sqrt{\frac{\sigma_{max} b_v^2}{4 A_c \rho C_D (\alpha h)^2 cos^2 \theta}}. \tag{9}$$

A higher critical orbital velocity indicates that the stem is more stable at a given location. Factors that contribute to stability are larger flexural strength (σ_{max}), smaller drag coefficient (C_D), and smaller correction factor (A_c). Further, vegetation parameters such as a large diameter (b_v), a small height ($h_v = \alpha h$), and a large leaning angle (θ) contribute to the stability by reducing the amount of wave force acting on the stem. The critical orbital velocity can be compared with an actual amplitude of the horizontal orbital velocity in the canopy, which is described by linear wave theory, based on water depth h, wave height H and wave period T via

$$u\left(z\right) = \frac{\omega H}{2} \frac{\cosh\left(k(z+h)\right)}{\sinh\left(kh\right)}, \tag{10}$$

where $\omega = 2\pi/T$ is the angular wave frequency (rad/s), z the distance from the water surface (positive upward), with $z = -h$ at the bottom (m), and k the wave number (rad/m). The comparison between critical and actual orbital velocity indicates if the stems will break under the local storm conditions. The set of equations to determine wave-induced and critical orbital velocities is referred to as the stem breakage model.

2.6 Implementation in a wave energy balance

Stems do not all break at the same wave conditions, as waves will predominantly break the weaker stems, see e.g. Rupprecht et al. (2017). Therefore, stem breakage will affect the stem density N_v, which subsequently influences wave energy dissipation by vegetation (Mendez and Losada, 2004). Stem breakage is applied to the quantification of wave height transformation over vegetated foreshores by means of a one-dimensional wave energy balance:

$$\frac{dEc_g}{dx} = -(\epsilon_b + \epsilon_f + \epsilon_v), \tag{11}$$

where $E = (1/8)\rho g H_{rms}^2$ is the wave energy density (J/m^2), $H_{rms} = H_{m0}/\sqrt{2}$ the root mean square wave height (m), c_g the group velocity, with which the wave energy propagates (m/s), x the distance along the transect (m), measured from the marsh edge, and on the right hand side wave energy dissipation (Jm^{-2}s^{-1}) due to wave breaking (ϵ_b), bottom friction (ϵ_f) and vegetation (ϵ_v).

For energy dissipation by breaking (ϵ_b), the formula of Battjes and Janssen (1978) is used, with the relation between the breaker index γ and the wave steepness according to Battjes and Stive (1985). Energy dissipation by bottom friction (ϵ_f) is described by the formulation of Madsen et al. (1988), where a relatively high Nikuradse roughness length scale of $k_N = 0.05$ m is used to account for the rough understory. Energy dissipation by vegetation (ϵ_v) is based on the formula of Mendez and Losada (2004). These model descriptions correspond with the selection of energy dissipation formulations in the spectral wave model SWAN (Booij et al., 1999). Along vegetated foreshores, wave energy is strongly related to the wave energy dissipation due to vegetation. This dissipation mechanism is dominant for the two salt marshes under consideration, even under storm conditions (Vuik et al., 2016). The formula for wave energy dissipation by vegetation of Mendez and Losada (2004) reads

$$\epsilon_v = \frac{1}{2\sqrt{\pi}} \rho C_D b_v N_v \left(\frac{kg}{2\omega}\right)^3 \frac{\sinh^3 k\alpha h + 3\sinh k\alpha h}{3k\cosh^3 kh} H_{rms}^3, \tag{12}$$

Here, it can be seen that vegetation parameters (b_v, N_v, h_v) affect the amount of wave energy dissipation. Stem breakage in particular affects the stem density N_v and height $h_v = \alpha h$, which is thus implemented in the wave energy balance, Eq. (11). The energy balance is discretized, using a simple first order numerical scheme with a grid cell size $\Delta x = 1.0$ m. The stem breakage model is evaluated in each computational grid cell. If the orbital velocity, Eq. (10), exceeds the stem's critical orbital velocity, Eq. (8) or (9), the stem height in the grid cell is reduced from h_v to a height of broken stems $h_{v,br}$. Such a reduction in stem height will subsequently influence the amount of wave height reduction.

The stem height reduction can be applied to all N_v stems per m^2 in the grid cell, solely based on the mean values for the vegetation characteristics. However, using single average values does not take into account the variation in strength, height and diameter of the stems, which leads to a fraction of broken stems (Rupprecht et al., 2017). Therefore, instead of using one deterministic value, a Monte Carlo simulation is performed in each grid cell by drawing 1000 random samples from the probability distributions of σ_{max}, h_v and b_v, taking into account the correlations between these 3 variables. The fraction of broken stems f_{br} is equal to the fraction of the 1000 samples in which $u > u_{crit}$. This approach leads to a mix of broken stems (stem density $f_{br}N_v$, stem height $h_{v,br}$) and standing stems (stem density $(1 - f_{br})N_v$, stem height h_v), see Fig. 7. The total wave energy dissipation by vegetation is equal to the sum of the contributions by standing and broken stems. This superposition of dissipation rates is based on

the assumption that orbital velocities in the bottom layer with broken stems are only weakly affected by the presence of the standing stems. This assumption is supported by the work of Weitzman et al. (2015), who found that the biomass of a low, secondary species in a multi-specific canopy significantly increases the attenuation of current- and wave-driven velocities.

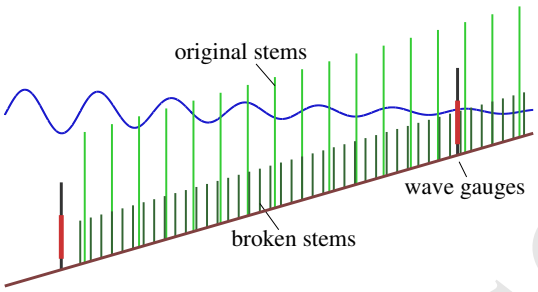

Figure 7: Schematization of the breakage process. The original vegetation is shown in green, broken stems in darker green. The positions of the two wave gauges are indicated in red. A uniform fraction of broken stems is applied.

A Gaussian distribution is applied for h_v and b_v, whereas a log-normal distribution is used for σ_{max} (Fig. 11). By choosing a log-normal distribution for σ_{max}, a positive number is guaranteed despite its large coefficient of variation (which is the ratio of standard deviation over mean value, σ/μ). In case of a small variation, the log-normal distribution resembles the Gaussian distribution. In addition, Pearson's correlation coefficients ρ between the 3 variables are incorporated to draw realistic combinations (Fig. 11). These correlation coefficients are determined for the sample locations close to the marsh edge and higher in the marsh separately. After that, the correlation coefficients are averaged over both sampling locations, and presented in this paper. This means that the correlation coefficients reflect the average in-sample co-variation. The dependencies between the variables are included by drawing 1000 random numbers between 0 and 1 from a Gaussian copula with correlation coefficients based on the samples, collected from the salt marshes. Realizations for h_v, b_v and σ_{max} are calculated by substituting the 1000 random numbers into the inverse probability distributions of these 3 variables.

2.7 Quantification of stem breakage in the field

In order to investigate the validity of the stem breakage model, the results of the model are compared with observations of the stem breakage process in the field. However, the available vegetation measurements have an insufficient frequency, accuracy and spatial extent to reveal the response of the stem density to wave action. This makes a one-to-one comparison between wave conditions and stem density reduction impossible. Alternatively, differences in stem density on the marsh are estimated from differences in wave attenuation. That means that the effect (wave attenuation) is observed, and the cause (stem density) is computed. Variations in wave attenuation are caused by variations in biomass on the salt marshes, since the bathymetry can be considered static at this time scale (see the limited difference in bed level in Fig. 1). As shown in Vuik et al. (2016), the presence of vegetation prevents wave breaking from occurring. Therefore, the observed differences in wave height reduction should be primarily attributed to differences in the vegetation on the marsh. The reconstructed variation of the stem density in time is used as data source in section 2.8, to calibrate the correction factor A_c in the stem breakage model, Eqs. (8) and (9).

The approach to compute the fraction of broken stems in the field is shown in the left part of the flow chart in Figure 8. The data underlying the analysis consists of the aforementioned wave data {1} and vegetation data {2}. The average wave height reduction over 50 m salt marsh is calculated for each month, for different combinations of water depth and wave height at the marsh edge {4}.

Before the wave energy balance can be applied, the drag coefficient C_D in Eq. (12) has to be defined {3}. The measured stem height, diameter and density for September 2015 are introduced in the model, for both sites and species. For the wave data, one period of non-stop wave measurements is used, from 16 July to 23 September 2015. A period of this length is required to include sufficient events with high waves in the time series. For each 15 minute time frame within this measurement period, the wave height reduction is modeled for a range of drag coefficients, from 0.0 to 5.0 with regular increments of 0.2. The drag coefficient in this range that leads to the best reproduction of the observed wave height reduction is selected, and related to the vegetation Reynolds number Re for the same 15 minute period. The vegetation Reynolds number is defined as follows, see e.g. Méndez et al. (1999):

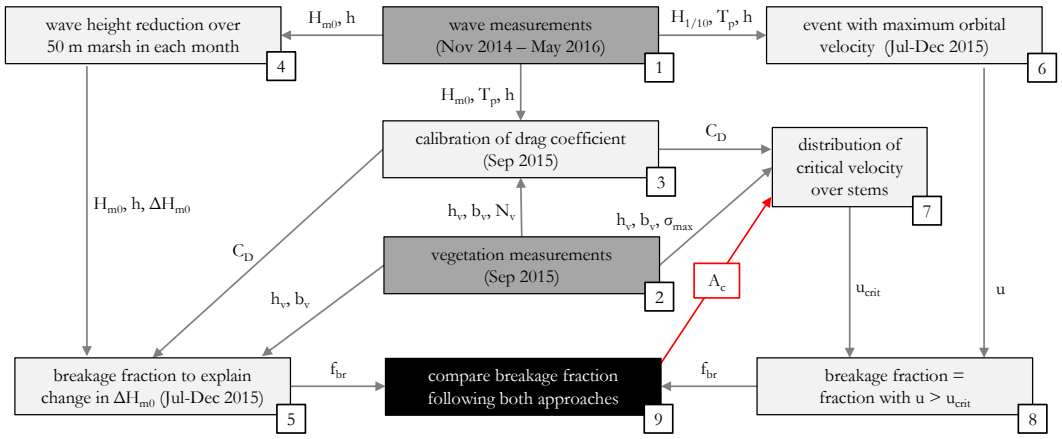

Figure 8: Flow chart of the approach to calibrate the stem breakage model, which explains how data sources (dark gray) and modeling steps (light gray) interact. Numbers in the flow chart refer to numbers {1} to {8} mentioned in the text. The aim of the calibration (black box) is to choose the correction factor A_c in such way, that the breakage fraction modeled with the stem breakage model {8} equals the breakage fraction based on observations of the wave attenuation in the field {5}.

$$Re = \frac{ub_v}{\nu}, \tag{13}$$

where u is the orbital velocity at the marsh edge, halfway up the stem height ($z = -h + h_v/2$), computed with Eq. (10), and ν is the kinematic viscosity of water ($\approx 1.2 \cdot 10^{-6}$ m^2/s). Finally, a relation between Re and C_D is determined. Following Méndez et al. (1999); Paul and Amos (2011); Hu et al. (2014) and others, the following type of equation is used:

$$C_D = a + \left(\frac{b}{Re}\right)^c, \tag{14}$$

in which the parameters a, b and c are found by non-linear curve-fitting. This equation is fitted through the (Re,C_D) combinations for all 15 minute periods.

The wave energy balance, Eq. (11), is used to determine a time-varying fraction of broken stems f_{br}, which leads to the best reproduction of the wave height reduction over the Hellegat

and Bath transects in each month {5}. The parameters stem height h_v, stem diameter b_v and the drag coefficient C_D according to Eq. (14) are based on the data set of September 2015, since this data is considered to be representative for the vegetation at the end of the summer. The data of September 2015 represents the properties of all stems, whereas the November 2015 or December 2014 samples only contain the subset of the stems that withstood the wave loads until November or December. The April 2015 data is not useful for this purpose, since the plants did not reach their full length yet. The bathymetry of November 2014 is included for both sites (Fig. 1). Vegetation does not change in height or diameter anymore from September onward. Therefore, the assumption is made that the vegetation in autumn consists of a mix of original long stems with September properties, and broken short stems, with a time-varying ratio between these two states.

The maximum wave height reduction occurs in summer, in June (*Scirpus*) or July (*Spartina*). It is assumed that all stems are standing upright at that time ($f_{br} = 0$), and the stem density N_v in these months is chosen in such way that the computed wave height reduction is equal to the measured reduction. For all other months, a fraction of this N_v stems is assumed to break, and a value $f_{br} > 0$ is computed for the 50 m salt marsh, to match the differences in wave height reduction throughout the year. These values of f_{br} are determined for each sea state of Table 1, and finally averaged over all sea states to obtain a robust value for each month.

A length of broken stems $h_{v,br}$ has to be specified to perform these computations. In December 2014, samples from *Scirpus* were collected near the marsh edge at Bath, where the vegetation was largely broken. 2/3 of the stems were lower than 20 cm, with a mean height of 10.4 cm. Therefore, $h_{v,br} = 0.10$ m is chosen for *Scirpus*. For *Spartina*, such samples were not available, but visual observations showed that this height is shorter than for *Scirpus* (see Fig 2). Therefore, a value of $h_{v,br} = 0.05$ m is selected. A sensitivity analysis has been carried out (not shown here), and the response of the correction factor A_c in the stem breakage model to a change of $h_{v,br}$ by a factor 2 was only 8%. So the exact choice of $h_{v,br}$ does not make a significant difference in case of *Spartina*.

2.8 Model calibration

The approach to calibrate the stem breakage model is shown on the right hand side of the flow chart in Figure 8. The reconstructed fraction of broken stems (left hand side of the flow chart) is used as data source for the calibration. The period from June (*Scirpus*) or July (*Spartina*) to

December 2015 is chosen for the calibration. June and July are the months with the maximum stem density, for which $f_{br} = 0$ is assumed. December 2015 was a relatively quiet month after a period with multiple storms in November, which had resulted in substantial (but not complete) stem breakage. Stems will break gradually during consecutive storm events. The standing stems at each point in time have a higher stability than required to withstand the most severe storm so far. Therefore, the total amount of broken stems in December 2015 is attributed to the event with the highest orbital velocity at 50 m in the marsh {6}. This event occurred on 28 November 2015 at Hellegat, with the following conditions at the marsh edge: $H_{m0} = 0.57$ m, $H_{1/10} = 0.72$ m, $T_p = 3.8$ s, $h = 3.0$ m, and the orbital velocity based on $H_{1/10}$ was $u = 0.52$ m/s. This orbital velocity is determined at halfway height of the stems. At Bath, the event with the highest orbital velocity occurred on 30 November 2015, with the following conditions at the marsh edge: $H_{m0} = 0.59$ m, $H_{1/10} = 0.75$ m, $T_p = 3.5$ s, $h = 1.6$ m, and $u = 0.79$ m/s.

In the right part of the flow chart, the stability-related vegetation characteristics, such as the flexural strength are introduced. The stems in the field vary in stability because of differences in length h_v, diameter b_v and flexural strength σ_{max}. This leads to a variation in the critical orbital velocity u_{crit} within the vegetation {7}, which is expressed in terms of a probability distribution. Correlation coefficients between stem height, diameter and strength are included to obtain a realistic distribution, as described before. The vegetation samples and three-point-bending tests from September 2015 are used for this purpose, for the same reasons as explained in section 2.7. The fraction of broken stems is equal to the fraction of stems for which $u_{crit} < u$ {8}. The drag coefficient in the equations is based on the Reynolds number at the marsh edge, using Eq. (14).

The hydraulic conditions in the selected event are applied as boundary conditions in the wave energy balance, at the marsh edge of Hellegat and Bath. In each grid cell, a fraction of broken stems f_{br} is determined, by comparing the local wave orbital velocity with the distribution of the critical orbital velocity. The wave attenuation in this grid cell is based on the sum of the contributions by $(1 - f_{br})N_v$ standing stems and $f_{br}N_v$ broken stems. Finally, one average value of f_{br} is determined over all grid cells in the 50 m long transects of Fig. 1 with salt marsh vegetation. This value is compared with the estimated fraction of broken stems based on the wave attenuation in December {9}. The value of the correction factor A_c is set at the point when the fractions of broken stems according to both approaches are identical.

Since the correction factors A_c are known after the calibration, a critical orbital velocity can

be determined for each sampled stem. The drag coefficient C_D in the expressions is determined iteratively via Eq (14) at $Re = u_{crit} b_v / \nu$. After that, a mean value and a standard deviation of u_{crit} are determined for each month with vegetation data.

2.9 Model validation

For model validation, the results of Rupprecht et al. (2017) for *Elymus athericus* (sea couch) are used. *Elymus* is a tall grass (70-80 cm), with thin stems (1-2 mm) and a high flexibility. The work of Rupprecht et al. (2017) was part of the Hydralab project, in which the interaction between salt marsh vegetation and waves was tested in a large-scale wave flume. Their paper gives a description of percentages of broken stems after several tests. For each tests, the statistics of the orbital velocity are available. Here, we validate the stem breakage model by comparing measured stem breakage fractions with the breakage fractions according to the stem breakage model. First, a mean and standard deviation of the critical orbital velocity are computed, based on the vegetation characteristics of the *Elymus*. After that, a breakage fraction is determined, which is the fraction of stems with a critical velocity lower than the mean value of the 10% highest orbital velocities ($u_{1/10}$, analogue to $H_{1/10}$), observed in the flume.

Since the flexible *Elymus* vegetation exhibits extreme leaning angles of more than 80 degrees, skin friction may significantly contribute to the forces on the plant. Form drag works over the reduced effective canopy height of roughly $h_{v,r} = 10$ cm, while a shear stress works over the full length h_v of the leaning stems (60-70 cm). Therefore, we add a friction term to the equations for the critical orbital velocity. The force due to friction equals

$$F_F = \frac{1}{2} C_f \rho u^2 A, \tag{15}$$

where A is the cylindrical surface area over which the friction works, which is $\pi b_v (h_v - h_{v,r})$. We schematize the forces acting on the vegetation as in Fig. 9, with a reduced vegetation height, and the higher part of the stems leaning horizontally in the flow. This schematization is based on photos of leaning *Elymus* in Rupprecht et al. (2017). These photos are also used to estimate that $h_{v,r} = 9$ cm in the situation just before the stems start to fold and break.

This results in an adaptation to the expression for the critical velocity, Eq (8), which reads

$$u_{crit,cir} = \sqrt{\frac{\sigma_{max} \pi \left(b_v^4 - b_{v,in}^4\right)}{8 A_c \rho b_v^2 \left[C_D h_{v,r}^2 + 2\pi C_f (h_v - h_{v,r}) h_{v,r}\right]}}, \tag{16}$$

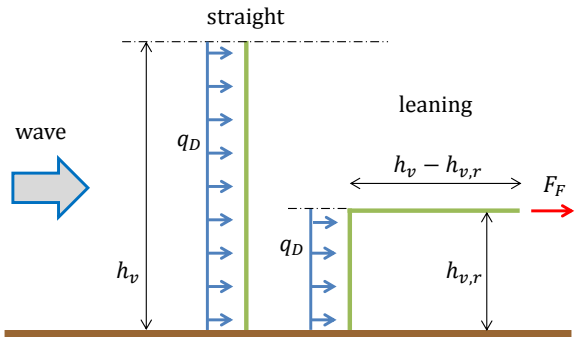

Figure 9: Schematized representation of forces working on *Elymus* at extreme leaning angles, with a drag force acting on a reduced canopy height $h_{v,r}$, and a shear stress working over the horizontal part of the stem, which results in a friction force F_F that works as a point load at height $h_{v,r}$.

where h_v is the full length (m) of the plant stems, $h_{v,r}$ is the reduced height (m) of the canopy after leaning and bending, and C_f is the friction coefficient, which is set to 0.01, as in Luhar and Nepf (2011).

Application of the relation between Reynolds number and drag coefficient as proposed in Möller et al. (2014) leads to a drag coefficient C_D in the order of 0.2-0.3. This is a bulk drag coefficient, which is based on wave model calibration. Its value is strongly influenced by the rigid cylinder approximation of the highly flexible vegetation, in which the full stem length is used as effective vegetation height. Therefore, this bulk drag coefficient is not representative for the maximum force that works on the vegetation. In this validation, C_D is set to 1.0, which is a characteristic value for drag forces on cylinders in wave motion (Hu et al., 2014).

From the considered plant species in this studies, the thinner and more flexible *Spartina* (EI≈2000 Nmm^2, see Table 3) comes closer to *Elymus* (EI≈300 Nmm^2, see Rupprecht et al. (2017)) than *Scirpus* (EI≈50,000 Nmm^2, see Table 4). Therefore, we apply the value of A_c that follows from the calibration for *Spartina*. Rupprecht et al. (2017) has presented the elasticity modulus E (2696 ± 1964 MPa) and flexural rigidity EI (299 ± 184 Nmm^2) of the stems, based on three-point-bending tests. However, the flexural strength σ_{max} (MPa) was not available. Therefore, we have analyzed the original data from these bending tests, and found that the flexural strength was 40 ± 28 MPa (sample size: 18 stems).

For each of the 18 sampled stems, the critical orbital velocity was computed using Eq. (16). This leads to a mean value and standard deviation of the critical orbital velocity. For each flume test, a mean and standard deviation of the measured orbital velocity is given in Rupprecht et al. (2017). Based on these normal distributions, a mean value is determined for the highest 10% of the orbital velocities ($u_{1/10}$). The computed fraction of broken stems f_{br} is equal to the fraction of stems for which the critical orbital velocity is lower than the actual orbital velocity $u_{1/10}$. These computed values are compared with the measurements of stem breakage.

3 Results

3.1 Seasonal variations in wave attenuation

The wave height reduction over the salt marsh varies over the seasons. A selection is made of 4 storm events that have occurred in summer and winter respectively, for which water depth and wave conditions at the marsh edge were nearly identical (Table 2). The ratio of wave height to water depth H_{m0}/h is chosen to illustrate the influence of vegetation on the wave height. For the storm of 25-07-2015 at Hellegat, H_{m0}/h decreases from 0.24 at gauge S1 (near the marsh edge) to 0.15 at gauge S4 (at 50 m in the marsh) due to the presence of dense *Spartina* vegetation (Vuik et al., 2016). In autumn (18-11-2015), this ratio is at S4 close to the value at S1, while in early spring (02-03-2016 and 26-04-2016), an increase over the salt marsh is visible, and the ratio of 0.31-0.33 approaches the limit for depth-induced wave breaking (e.g., Nelson (1994)). These results show a clear seasonal difference, as the greater decrease in this ratio in summer signifies stronger wave attenuation by vegetation. The same pattern is visible for *Scirpus* at Bath. In late spring, the wave height to water depth ratio at gauge S4 (19-05-2015, 0.07) is approximately half of this ratio in any other season (0.12-0.15).

Storm events such as in Table 2 do not occur in every month. Therefore, less energetic sea states were selected to analyze seasonal variations in wave attenuation for comparable wave height and water depth. Fig. 10 shows how the wave height reduction varies over the months at Hellegat (top panel) and Bath (lower panel).

The highest wave attenuation by *Spartina* at Hellegat (Fig. 10a) was observed in summer, roughly from May to September. In autumn and winter, the wave attenuation gradually decreased from September to a minimum in March. In spring, new shoots started growing, leading to a rapid increase in wave attenuation from March to May. The salt marsh at Bath with *Scir-*

Table 2: Seasonal variations in the ratio of significant wave height H_{m0} over water depth h at gauge S4, 50 m in the salt marsh, for 4 events with nearly identical water level ζ, water depth h, significant wave height H_{m0} and wave peak period T_p at gauge S1 at Hellegat (top) and Bath (bottom).

date		25-07-2015	18-11-2015	02-03-2016	26-04-2016
ζ (S1)	m+NAP	2.57	2.57	2.57	2.58
h (S1)	m	1.97	1.99	1.97	1.95
h (S4)	m	0.73	0.69	0.72	0.76
H_{m0} (S1)	m	0.47	0.48	0.46	0.47
H_{m0} (S4)	m	0.11	0.16	0.22	0.25
T_p (S1)	s	3.18	3.18	2.99	2.83
H_{m0}/h (S1)	-	0.24	0.24	0.23	0.24
H_{m0}/h (S4)	-	0.15	0.23	0.31	0.33

date		23-12-2014	19-05-2015	28-11-2015	26-04-2016
ζ (S1)	m+NAP	3.40	3.43	3.44	3.44
h (S1)	m	1.49	1.52	1.49	1.53
h (S4)	m	0.73	0.76	0.76	0.75
H_{m0} (S1)	m	0.27	0.28	0.30	0.27
H_{m0} (S4)	m	0.11	0.05	0.09	0.09
T_p (S1)	s	2.44	2.18	2.18	2.56
H_{m0}/h (S1)	-	0.18	0.18	0.20	0.18
H_{m0}/h (S4)	-	0.15	0.07	0.12	0.12

pus (Fig. 10b) showed similar trends as that of Hellegat, but because of the smaller number of inundations, the results of Fig. 10b have larger variations than Fig. 10a. The minimum wave height reduction was found in winter, in the months January, February and March.

3.2 Seasonal variations in vegetation characteristics

The vegetation characteristics demonstrate a seasonal dependence as can be seen in Tables 3 and 4. Only standing stems were sampled, regardless of the presence of broken or folded stems at some points in time.

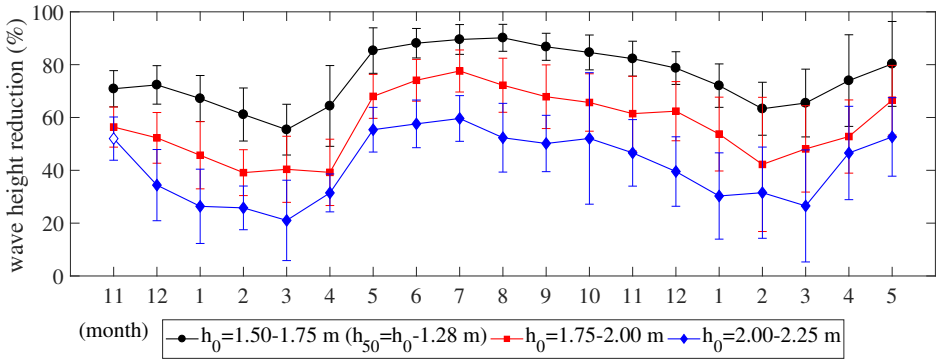

(a) Hellegat

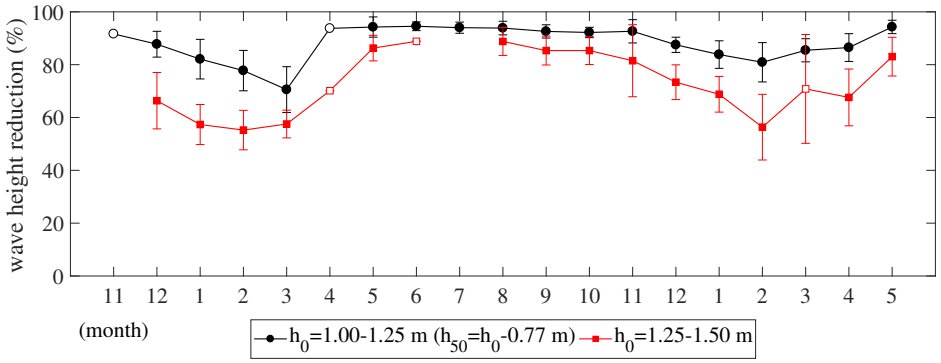

(b) Bath

Figure 10: Monthly average wave height reduction $(H_{s,0} - H_{s,50})/H_{s,0}$ (%) over 50 m salt marsh between wave gauges S1 and S4 at Hellegat (top panel) and Bath (lower panel) for the period Nov 2014 - May 2016, for an incoming significant wave height between 0.1 and 0.2 m, combined with a water depth at the marsh edge h_0 as shown in the legends. Open markers indicate that less than 5 occurrences were available in that month to compute the average reduction. Error bars give the mean value plus and minus one standard deviation.

In April, new shoots were measured, as can be seen from the relatively low stem height of 285 (*Spartina*) and 399 mm *Scirpus*. For both species, the diameter and height of the stems is larger in September than in April. In November, the flexural strength is much higher than in September, especially for *Spartina* (8.8 MPa in September, 17.0 MPa in November). This might be caused by breakage of stems with a lower flexural strength, but evidence is lacking to support this hypothesis. A statistically significant difference is found (t-test, p=0.002) between the flexural strengths of both species, with a higher mean strength of *Spartina* (12.5 MPa) compared to

Table 3: Characteristics of *Spartina anglica* (mean value ± standard deviation) per measurement period.

Period		Dec 2014	Apr 2015	Sep 2015	Nov 2015	All
Samples		25	20	20	20	85
h_v	mm	327 ± 125	285 ± 63	544 ± 111	608 ± 50	441 ± 87
b_v	mm	3.1 ± 0.5	3.3 ± 0.5	4.1 ± 0.9	3.7 ± 0.5	3.5 ± 0.6
σ_{max}	MPa	13.9 ± 7.0	10.4 ± 5.1	8.8 ± 4.6	17.0 ± 5.8	12.5 ± 5.6
E	MPa	708 ± 560	318 ± 178	224 ± 151	503 ± 198	438 ± 272
EI	Nmm^2×10^3	2.0 ± 1.0	1.6 ± 0.5	2.5 ± 1.6	2.3 ± 1.1	2.1 ± 1.0
$\rho(h_v, b_v)$		0.29	0.43	0.70	0.25	0.42
$\rho(h_v, \sigma_{max})$		0.21	-0.11	-0.20	0.59	0.13
$\rho(b_v, \sigma_{max})$		-0.74	-0.09	-0.40	0.03	-0.30

Table 4: Characteristics of *Scirpus maritimus* (mean value ± standard deviation) per measurement period.

Period		Dec 2014	Apr 2015	Sep 2015	Nov 2015	All
Samples		20	20	19	19	78
h_v	mm	737 ± 169	399 ± 178	1015 ± 175	738 ± 208	722 ± 183
b_v	mm	6.8 ± 1.5	7.6 ± 1.9	8.0 ± 1.7	6.8 ± 1.4	7.3 ± 1.6
σ_{max}	MPa	6.8 ± 2.5	8.5 ± 4.1	9.5 ± 4.4	11.8 ± 6.2	9.2 ± 4.3
E	MPa	1130 ± 305	1625 ± 1120	917 ± 600	2052 ± 946	1431 ± 743
EI	Nmm^2×10^3	43 ± 29	58 ± 44	54 ± 35	51 ± 33	52 ± 35
$\rho(h_v, b_v)$		0.43	0.35	0.24	-0.02	0.25
$\rho(h_v, \sigma_{max})$		-0.40	0.04	0.16	-0.04	-0.06
$\rho(b_v, \sigma_{max})$		-0.06	-0.35	-0.64	-0.62	-0.42

Scirpus (9.2 MPa). A flexural strength of 12 ± 7 MPa was reported for *Spartina alterniflora* in Feagin et al. (2011), which is in the same range as the flexural strength of the *Spartina anglica* in the current study. The correlation coefficients provide some additional information. They show that for both species, longer stems are generally thicker (positive ρ), and thicker stems tend to have a lower strength (negative ρ, see Fig. 11 for *Scirpus*). The latter observation is in line with Feagin et al. (2011), who found indications of an inversely proportional relationship

between stem diameter and flexural strength of *Spartina alterniflora*.

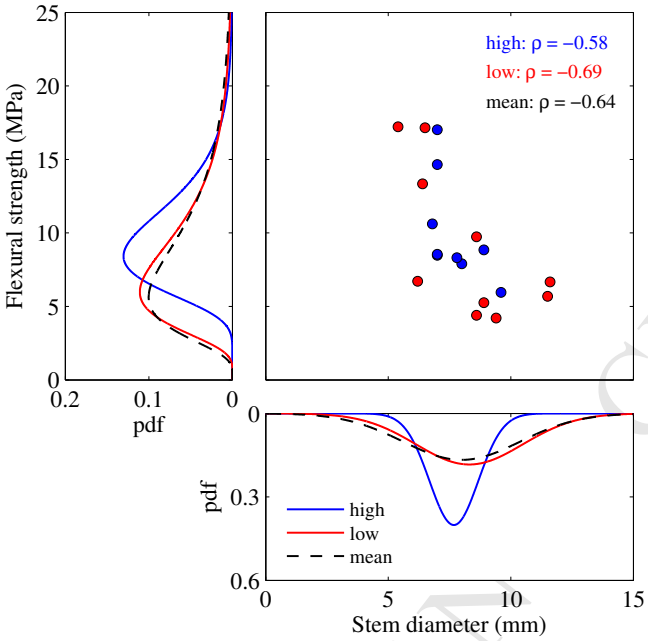

Figure 11: Example of the stem diameter b_v and flexural strength σ_{max} for individual stems, their probability density functions, and the correlation coefficient between these variables, for *Scirpus* samples from September 2015 at Bath, with sample locations close to the marsh edge ('low') and higher in the marsh ('high').

In September 2015, a detailed stem density measurement was carried out. The mean stem density was 934 stems/m^2 for *Spartina* at Hellegat (842 and 1027 for the two individual locations), and 360 stems/m^2 for *Scirpus* at Bath (352 and 368 for the two individual locations).

3.3 Seasonal variations in fraction of broken stems

Seasonal variations in the fraction of broken stems are computed based on the seasonal variations in wave attenuation (Fig. 10), using the one-dimensional wave energy balance, Eq. (11). Figure 12 shows the relation between C_D and Re for both field sites. Fitting parameters of Eq. (14) are for Hellegat $a = 0.00$, $b = 943$, and $c = 0.48$, and for Bath $a = 1.59$, $b = 461$, and $c = 1.25$. The relatively high drag coefficient of *Scirpus maritimus* is related to the large frontal plant area

with many leaves (Heuner et al., 2015). This relation between C_D and Re is used to reconstruct vegetation properties based on the measured wave attenuation.

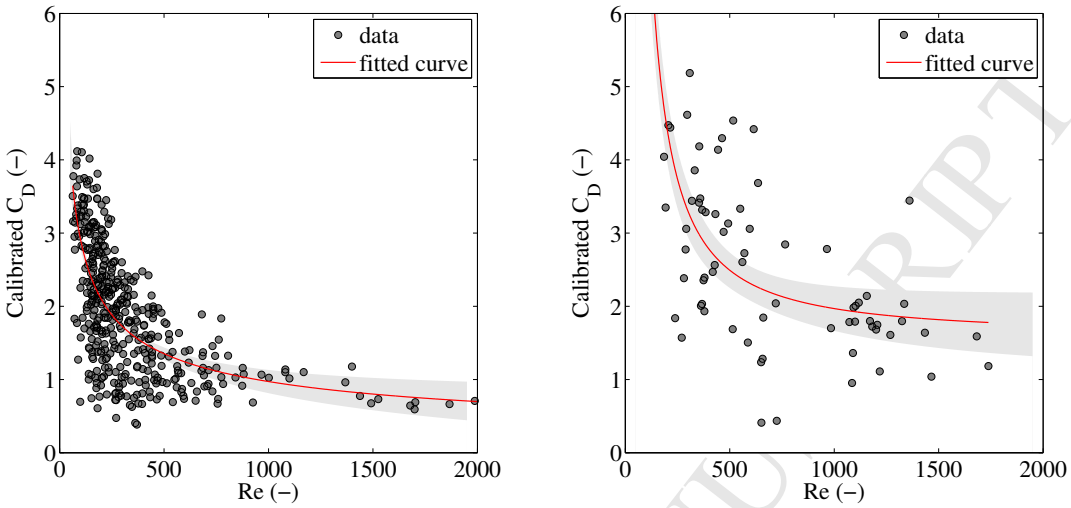

(a) Hellegat (b) Bath

Figure 12: The relationship between calibrated bulk drag coefficients C_D and the corresponding Reynolds numbers Re for Hellegat (left) and Bath (right), and its 95% confidence interval (shaded area). Re is based on the hydrodynamics at the marsh edge. The curve is given by Eq. (14).

The maximum wave height reduction occurs in summer, in July (*Spartina*) or June (*Scirpus*). With the drag coefficient, stem height and stem diameter as known variables, the wave energy balance is applied to determine the unknown maximum stem density: 1190 stems/m^2 (*Spartina*) and 850 stems/m^2 (*Scirpus*), assuming that $f_{br} = 0$ at that time. The lower wave height reduction in the other months is caused by breakage of a part of the stems ($f_{br} > 0$, see Fig. 13). In September, the computed number of standing stems per m^2 was 950 stems/m^2 (*Spartina*) or 400 stems/m^2 (*Scirpus*). This is close to the measured values of 930 and 360 stems/m^2, respectively. The computed breakage fractions for December 2015 are equal to 0.52 (*Spartina*) and 0.85 (*Scirpus*). These values will be compared with the results of the stem breakage model, as indicated in the flow chart (Fig. 8).

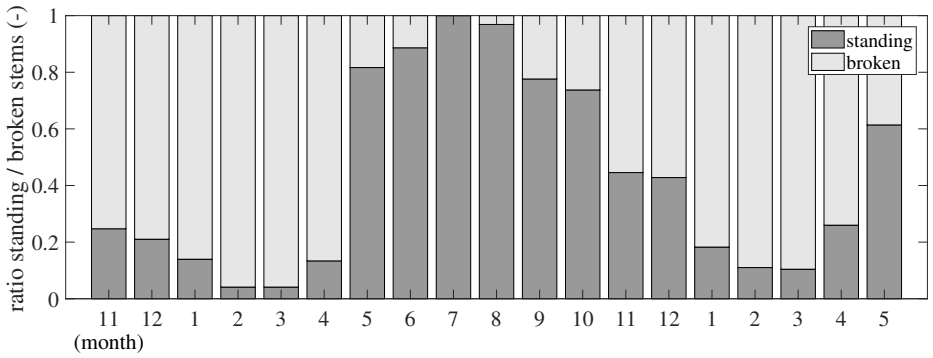

(a) Hellegat

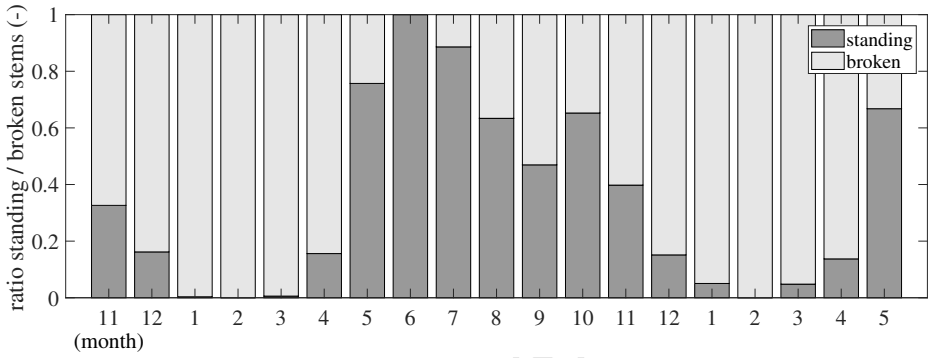

(b) Bath

Figure 13: The computed proportion of standing (1-f_{br}) and broken (f_{br}) stems for each month in the period November 2014 - May 2016, based on observations of wave attenuation.

3.4 Model calibration

The performance of the stem breakage model is optimized by calibrating the correction factor A_c for wave-induced bending stress in the Equations (8) and (9). Following the right hand side of the flowchart in Fig. 8, a fraction of broken stems is computed with the stem breakage model, which is implemented in the wave energy balance. The distribution of the critical orbital velocity is based on the vegetation data of September 2015 in Tables 3 and 4, including the correlation coefficients. The computed fraction of broken stems depends on A_c (Fig. 14). The stem density for A_c=0 (no breakage) represents the situation with a breakage fraction $f_{br} = 0$, which is assumed to be in July 2015 (*Spartina*) or June 2015 (*Scirpus*), see Figs. 13a and 13b. The dashed lines in Fig. 14 indicate the fraction of broken stems in December 2015, and the correction factors that lead to

these fractions. The stem density reduction from summer to December 2015 is best reproduced with A_c=1.7 for *Spartina* and A_c=1.3 for *Scirpus*.

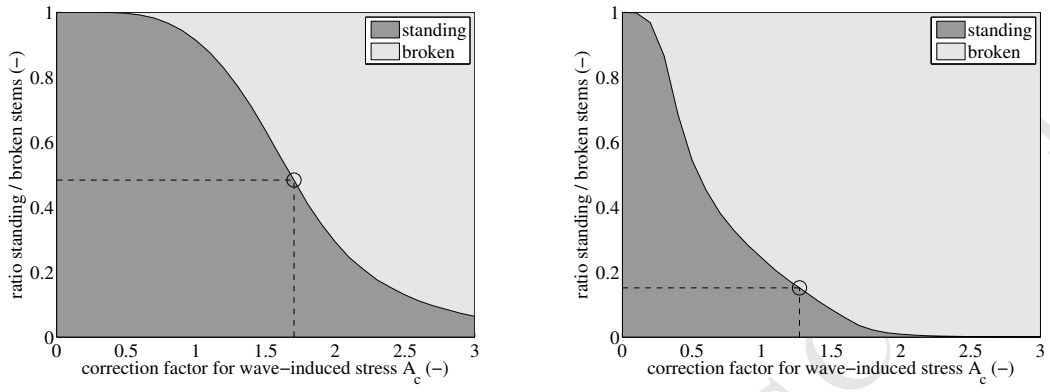

(a) Hellegat (b) Bath

Figure 14: The fraction of broken stems f_{br} for *Spartina anglica* at Hellegat (left) and *Scirpus maritimus* at Bath (right), computed with the stem breakage model, as a function of the correction factor A_c.

Stems break when the wave orbital velocity exceeds the critical orbital velocity u_{crit} of the vegetation, which is a measure for the stability of the stems. This velocity is determined for each sampled stem, including the calibrated correction factors A_c in the equations (Table 5).

In general, *Spartina* (u_{crit}=0.86 ± 0.28 m/s) is significantly (t-test, p=0.0003) more stable than *Scirpus* (u_{crit}=0.59 ± 0.22 m/s), which is also in agreement with visual observations, see Fig. 2. The stability of *Spartina* is relatively high in December 2014 and April 2015. This is related to the short stems, measured in these months (Table 3). In November, the plants are most vulnerable to stem breakage, with a critical orbital velocity of 0.52 ± 0.09 m/s. Assuming a normal distribution, we see that the most stable 2.5% of the stems breaks at an orbital velocity of 0.70 m/s. The stability of newly growing *Scirpus* plants (April 2015) is quite high (u_{crit}=0.99 ± 0.38 m/s), because the plants have not reached their full length (399 mm in April, 1015 mm in September, Table 4), which is squared in Eq. (9). In other months, the tall plants are highly vulnerable to stem breakage, with breakage of the full-grown September vegetation already occurring for orbital velocities of 0.30 ± 0.05 m/s, with breakage of the 2.5% most stable stems at 0.40 m/s.

Table 5: Computed critical orbital velocity (m/s) for the sampled stems of Tables 3 and 4, mean value ± standard deviation.

Species	Period	u_{crit}
Spartina anglica	2014 Dec	1.19 ± 0.60
	2015 Apr	1.14 ± 0.31
	2015 Sep	0.58 ± 0.13
	2015 Nov	0.52 ± 0.09
	All	0.86 ± 0.28
Scirpus maritimus	2014 Dec	0.51 ± 0.27
	2015 Apr	0.99 ± 0.38
	2015 Sep	0.30 ± 0.05
	2015 Nov	0.56 ± 0.19
	All	0.59 ± 0.22

3.5 Model validation

The critical orbital velocity of *Elymus athericus*, according to Eq. (16), is 1.06 ± 0.34 m/s. When neglecting friction, and using Eq. (8), this value increases to 1.28 ± 0.41 m/s. This means that the effect of skin friction decreases the critical orbital velocity by 17%.

Table 6: Observed orbital velocities, computed mean value of the 10% highest orbital velocities ($u_{1/10}$), and observed and computed stem breakage fractions f_{br}.

Test	u (m/s)	$u_{1/10}$ (m/s)	f_{br} (-) observed	computed
10	0.48 ± 0.07	0.61	>0	9%
14	0.83 ± 0.17	1.14	45%	59%
15	0.95 ± 0.10	1.13	80%	58%

Observed orbital velocities, and observed and computed stem breakage percentages are summarized in Table 6. Stems started to fold in test 10 from the Hydralab experiments, with medium orbital velocities (0.48 ± 0.07 m/s). The stem breakage model computes that 9% of the stems will fold or break in this test, which means that the threshold of stem folding is correctly predicted by the model. 45% of the stems were broken after test 14, with high orbital velocities

(0.83 ± 0.17 m/s). The stem breakage model gives 59% stem breakage under these conditions, which is higher than the measured amount. The highest mean orbital velocity was generated in test 15 (0.95 ± 0.10 m/s). After this test, 80% of the stems were broken. The stem breakage model gives only 56% stem breakage. This is because the model uses $u_{1/10}$, which is smaller in test 15 compared to test 14, because of the relatively high standard deviation in test 14. Model results (58%) and measurements (80%) deviate here, which will be evaluated in the discussion section.

3.6 Application to a schematic salt marsh

This section gives an illustrative application of the calibrated stem breakage model for a schematic salt marsh with *Spartina anglica* (Fig 15). Vegetation characteristics of September 2015 are applied (Table 3). An arbitrary initial stem density of 1000 stems/m^2 is chosen. The bottom consists of a sloping part of 200 m from 2.0 to 3.0 m+MSL, followed by a flat part of 300 m at 3.0 m+MSL, further landward. Storm conditions are applied with a water level at 5.0 m+MSL, with an incident significant wave height of 1.0 m and a peak period of 4.0 s. That means that the water depth is 3.0 m at the seaward boundary, and 2.0 m above the flat part of the salt marsh. There is no wind input active, so only dissipative mechanisms play a role.

Without vegetation, the processes of depth-induced wave breaking and bottom friction lead to a wave height reduction of roughly 6% at 200 m and 25% at the landward end of the salt marsh. Addition of fully stable vegetation leads to a rapid decline in wave height, up to 97% at 500 m. The stem breakage model predicts breakage over 450 m, when solely based on mean values for the vegetation characteristics, for which all stems in each grid cell either stand or break. Further landward of this point, the original vegetation is undamaged (bimodal behavior). The 100% broken vegetation seaward of this point leads to some additional dissipation with respect to the case without vegetation. Alternatively, when computing a fraction of broken stems in each computational grid cell, based on the variation in vegetation characteristics, the stem breakage gradually decreases from 92% at the marsh edge to nearly 0% at 300 m and further landward. The partially broken vegetation leads to wave energy reduction, and reduces the wave loads on the vegetation further landward. The two stem breakage approaches lead to different wave height reduction (difference in wave height up to 0.4 m), especially over the part of the marsh where the mean value approach leads to full breakage.

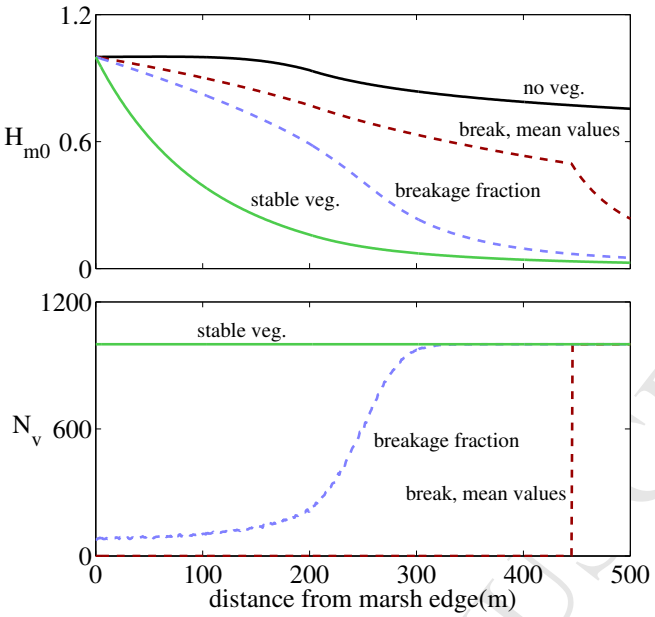

Figure 15: Reduction in significant wave height H_{m0} (m) (upper panel) and stem density N_v (stems/m^2) (lower panel) for a *Spartina* marsh, which consists of a sloping part of 250 m and a flat part of 250 m. The curves show the computational result when applying no vegetation, stem breakage with mean values only, the approach with a fraction of broken stems, or stable vegetation.

4 Discussion

In this study, a model has been presented that determines the wave-induced forces that lead to vegetation stem breakage. Rupprecht et al. (2015) recommended studying both plant morphology (height and diameter) and mechanic characteristics when considering plant stability. The stem breakage model proposed in this paper combines these two factors into an expression for a critical orbital velocity (Eqs. (8) and (9)). Three-point bending tests were utilized to investigate seasonal variability in flexural strength. Previous work only considered the strength of plants in its summer state, and recommended to measure the variability in mechanical properties due to differences in the stage of life cycle or vitality of plant stems (Rupprecht et al., 2015). The current study explicitly examines the seasonal variation in stem strength. We hypothesize that the presented strength variations are the result of a combination of internal biological processes

and wave action that filters out the relatively weak plants.

Quantifying the thresholds of stem breakage is extremely challenging due to the complicated interaction between wave motion and vegetation motion, mechanical stresses due to dynamic wave loads in the swaying vegetation, and temporal and spatial variability in plant characteristics. The model proposed in this paper simplifies this complicated process by combining linear wave theory and formulas from static mechanics. In spite of this simplification, the model captures the essence of the stem breakage process, as can be seen from the calibrated correction factors A_c (1.7 for *Spartina* and 1.3 for *Scirpus*), which are in the order of 1. Several assumptions and choices can lead to such a deviation from 1. We distinguish between (1) assumptions and simplifications where the model concept and its parameters are based on, and (2) assumptions and choices that were made in the procedure to calibrate the model.

The first category of assumptions is related to the model concept and the definition of its parameters.

- Orbital velocities in the model are based on linear wave theory (Mendez and Losada, 2004), while in-canopy velocities are known to decrease in dense canopies (Luhar et al., 2010). This means that stems may break for lower actual in-canopy velocities than the critical orbital velocities presented in this paper.

- Another assumption is the choice of $H_{1/10}$, implying that the mean height of the highest 10% of the waves determines whether the vegetation breaks or not. No information is available to investigate which individual wave in the random wave field causes the vegetation to break. $H_{1/10}$ is one of the many options to describe the upper tail of the wave height distribution. Selection of a higher characteristic value from the wave height distribution would directly lead to a lower required A_c.

- Ship waves can also cause high wave loads at small water depths, which was specifically described for Bath by Schroevers et al. (2011). Such individual waves are not included in the wave spectra and in $H_{1/10}$.

- Further, the leaning angle θ strongly influences the results. Stem bending was approximated by a constant leaning angle, which was based on a single experiment for each of the species. The selected value of 30 degrees for *Scirpus* was based on interpolation between measurements of leaning under low- and high-frequency wave forcing (Silinski et al., 2015).

A sensitivity analysis (not presented) shows that the correction factor A_c reduces from 1.3 to 1.1 for an angle of 20 degrees, and increases to 1.6 for an angle of 40 degrees. A higher leaning angle reduces the flexural stress in the stems, and would require a higher value of A_c to obtain the same amount of stem breakage. Estimation of a leaning angle for different plant species requires mechanistic understanding of the relationship between wave properties, flexural rigidity EI and stem leaning.

- Finally, the correction factor A_c also accounts for processes that are not explicitly included in the stem breakage model, for instance the effects of dynamic loading (de Langre, 2012), fatigue due to repeated wave loads (Mach et al., 2007) and crowding, where neighboring plants provide physical support (Harley and Bertness, 1996). Further research is needed to determine whether these processes are influential.

The second category of assumptions that influence the model outcomes is related to the calibration procedure.

- Seasonal variations in wave attenuation were used to estimate the corresponding variations in the fraction of broken stems on the salt marshes, because in-situ vegetation measurements were not sufficient to assess the response to wave forcing. This is why the effect (wave attenuation) has been observed, and the cause (the number of standing and broken stems) has been computed. The computed fraction of broken stems was used as data source for the calibration of the model.

- Several choices and assumptions were made in reconstructing the seasonal variations in the fraction of broken stems, such as the length of broken stems and the selection of sea states (depth-wave height combinations). We have tested that application of a length of broken *Spartina* stems of 0.10 m instead of 0.05 m leads to a limited increase in A_c of 8%.

- Further, C_D was calibrated for vegetation data from September 2015 only, while seasonal differences, for instance in stem flexibility and amount of leaves, could lead to seasonal variations in C_D. The flexibility EI of both species in Sep. 2015 and Nov. 2015 is similar (Tables 3 and 4). A possible decrease in amount of leaves leads to a decrease in C_D in autumn, and a lower fraction of broken stems than shown in Fig 13. Such a decrease in computed stem breakage leads to a decrease of A_c (Fig. 14).

- Wave energy dissipation by standing and broken stems is summed up to obtain a total dissipation rate. This approach is based on the assumption that orbital velocities in the

bottom layer with broken stems are only weakly affected by the presence of the standing stems. This is in line with the application of linear wave theory in Mendez and Losada (2004) and is supported by the findings of Weitzman et al. (2015) for a canopy composed of a tall upperstory and a short understory. For sparse standing vegetation or low-density canopies, this approach is valid. For high density vegetation, the wave orbital velocities in the broken vegetation may be lower than predicted by equations from linear wave theory. This effect could be taken into account via a reduced drag coefficient C_D for the broken fraction. On the other hand, the drag coefficient of short, broken stems may be higher, since they act as short, stiff cylinders (Hu et al., 2014). Detailed measurements on the complex interaction between the waves and the mix of broken and standing vegetation were not carried out. Therefore, for reasons of simplicity, the same drag coefficient was applied for both fractions.

Validation of the calibrated model ($A_c = 1.7$) was performed, using observations of stem breakage of *Elymus athericus* in a wave flume (Rupprecht et al., 2017). The very high flexibility of *Elymus* increases the complexity of the vegetation-wave interaction significantly. Nonetheless, the model was able to predict the initiation of stem breakage correctly. Rupprecht et al. (2017) gives two measurements of stem breakage: 45% after day 8 (test 14), and an additional 35% after day 10 (test 15, 80% in total). Where the first measurement was reproduced with reasonable accuracy (59%), the 80% of stem breakage after day 10 was not correctly reproduced (58%). Modeled fractions are based on the mean value of the 10% highest orbital velocities ($u_{1/10}$). This quantity does apparently not reflect the main differences between both tests.

A possible reason for the increase in breakage fraction is the long time span of 11 days over which wave tests were performed. The mechanical properties of the canopy after several days of testing may differ from the properties that were determined before the tests were performed. Another aspect is the extremely high non-linearity of the waves in the tests on day 11, with waves of 0.9 m at a water depth of 2.0 m and a substantial difference between forward and backward orbital velocity. Possibly, high turbulence levels have contributed to additional stem breakage. Further, a time lag up to 90° exists between wave orbital motion and vegetation motion (Rupprecht et al., 2017). This may lead to high bending moments in the stage before maximum leaning, which is not included in the model. We conclude that the stem breakage model did a reasonable job in reproducing the observed stem breakage, with the notion that the simplified description of waves and mechanics may lead to deviations, especially in situations

with complex hydrodynamics and vegetation motion.

The number of measurements of stem breakage is still very limited. The reliability of the model predictions could be investigated further if additional measurements would be performed. Useful validation data could be obtained by frequent measurements of the fraction of broken stems, by in-situ measurements, or by application of non-destructive methods such as time-lapse photography or satellite images (e.g., O'Donnell and Schalles (2016)). Preferably, several pre- and post-storm measurements should be carried out. These measurements should include vegetation characteristics (stem height, diameter and density) and flexural strength measurements by means of three-point bending tests. This should be combined with wave measurements during the storm. Alternatively, large-scale flume experiments as described in Rupprecht et al. (2017) can provide additional information for validation, if accompanied with measurements of the mechanical properties of the vegetation. In flume experiments, stem breakage can be more accurately linked to stem breakage, compared to field measurements.

Remarkable differences were visible between the two considered plant species, *Spartina anglica* and *Scirpus maritimus*. The relative change in A_c to reduce f_{br} from 90 to 10% is 50% larger for *Spartina*, compare the slopes of Figs. 14b and 14a. That implies that *Scirpus* is more sensitive to the magnitude of wave-induced stresses than *Spartina*. The same conclusion follows from the computed critical orbital velocities (Table 5). *Scirpus* requires a location with a relatively mild wave climate, or when another species attenuates the waves to a certain extent, and provides a sheltered habitat further up the marsh (Heuner et al., 2015). The aforementioned pre- and post-storm measurements could help in determining the causes of the decline in biomass, including stem breakage by storm waves, stem breakage by fatigue (especially *Spartina* at Hellegat is frequently inundated and exposed to waves), and biological processes such as changing mechanical properties of the plants in autumn.

The partial stem breakage, observed in the wave flume tests of Rupprecht et al. (2017), indicates that individual *Elymus* stems vary in stability. This was also found in the current study for *Spartina* and *Scirpus*. From the 3 considered species, the flexible *Elymus* has the highest stability (u_{crit} =1.06 $\pm$ 0.34 m/s), whereas full-grown tall and stiff *Scirpus* is most vulnerable to stem breakage (u_{crit} =0.30 $\pm$ 0.05 m/s, September), with *Spartina* in between (u_{crit} =0.58 $\pm$ 0.13 m/s, September).

The critical orbital velocity as computed by the stem breakage model can be used for a first

estimate of the (relative) stability of other plant species, provided that vegetation characteristics (height, diameter) and flexural strength are known. For such an estimate, preliminary values for A_c, C_D and θ can be used, with A_c between 1.0 and 2.0, in combination with a value for θ that reflects the flexibility of the considered plants. For the drag coefficient C_D, a value should be chosen that represents actual drag forces on the plants. Especially for highly flexible vegetation, this value may be substantially higher than a bulk drag coefficient that follows from calibration of a wave model. For a more quantitative description of the stem breakage of different plant species or locations, plant species-specific validation is recommended.

This paper has shown how the stem breakage model can be implemented in a wave model such as a spectral wave model or a simple wave energy balance, to incorporate stem breakage in simulations of wave loads on dikes with a vegetated foreshore. The wave load reduction on the flood defense due to vegetation decreases when stem breakage occurs, and declines in extreme cases to a situation where all vegetation is broken. Such extreme cases are equivalent to a wave flume test with completely mowed vegetation described in Möller et al. (2014), for which still some wave height reduction was measured. Including the variability in individual stem stability prevents bimodal model behavior, in which all stems either break or stand. Partial stem breakage leads to partial wave attenuation reduction. This results in a gradual decrease in wave-induced forces and, subsequently, in a gradual decrease in the fraction of broken stems, for increasing distance from the marsh edge. In this way, the role of vegetation can be more realistically included in flood risk assessments.

5 Conclusions

Wave measurements at two salt marshes revealed a strong seasonal variation in wave attenuation by salt marsh vegetation. Common cord-grass (*Spartina anglica*) and sea club-rush (*Scirpus maritimus*) were used as study species. From field observations and an analysis of the seasonal variation in wave attenuation, the above-ground biomass of these species was found to gradually diminish during the storm season (October to March in the Netherlands). At the end of winter, typically only a rough salt marsh bottom with remainders of folded and broken vegetation is present. From April onwards, new shoots start to grow, which eventually develop to dense vegetation with high wave damping capacity in summer.

Seasonal variations in biomass are caused by seasonal differences in storm intensity and

mechanical properties of the stems. The stem height, stem diameter and flexural strength were measured for four measurement periods in the seasonal cycle, where the strength was determined by means of three-point bending tests. Both study species have their maximum flexural strength in the winter period. The stems of *Scirpus* have a lower flexural strength than that of *Spartina*.

A new model is presented in this paper, which predicts the wave load that plant stems can withstand before they break or fold. The model compares plant stability, expressed in terms of a critical orbital velocity, Eqs. (8) and (9), with the amplitude of wave-induced orbital velocities in the canopy, Eq. (10). A higher critical velocity indicates greater stability of the stem. Factors that contribute to stability are a high flexural strength and large stem diameter. Further, vegetation characteristics such as a small stem height, low drag coefficient and high flexibility (i.e., a large leaning angle) contribute to the stability, by reducing the amount of wave force acting on the stem. The model was calibrated, based on continuous measurements of water depth and wave conditions, over a period of 19 months. A correction factor in the stem breakage model (1.7 for *Spartina* and 1.3 for *Scirpus*) was required to reproduce the amount of stem breakage that occurred in the field. An independent validation of the model was carried out, by comparing model predictions of stem breakage of sea couch (*Elymus athericus*) with observations of Rupprecht et al. (2017) in a large-scale flume experiment with wave heights up to 0.9 m. The stem breakage model correctly reproduced the starting point of folding. An observation of 45% stem breakage at high orbital velocities was reproduced with reasonable accuracy (57%). During the flume test with the highest orbital velocities, 80% stem breakage was observed, whereas the model predicted that 56% would break.

Spartina is relatively stable with a mean critical orbital velocity in the order of 0.5-1.2 m/s. The stability of *Scirpus* is lower, because of its smaller strength, lower flexibility and longer stems, with a mean critical orbital velocity of 0.3-1.0 m/s. These velocities are based on $H_{1/10}$, which is the mean height of the highest 10% of the waves. The stem breakage model was implemented in a wave energy balance to combine the calculations of wave attenuation and stem breakage. If the variation in individual stem properties is taken into account, a spatially varying fraction of broken stems can be calculated. In this way, bimodal model behavior is prevented, in which all stems either stand or break.

The stem breakage model can be used to predict the amount of remaining biomass on vegetated foreshores under design conditions for dikes. As a process-based model, it can be applied

to different plant species and locations, provided that the characteristics (height and diameter) and flexural strength of the plants are determined. If possible, it is preferred to carry out a species-specific validation. Omitting stem breakage will lead to an overestimation of wave height reduction, while application of the stem breakage model will lead to a more realistic assessment of the role of vegetation for coastal protection.

Table 7: List of variables

Symbol	Name	Units
α	Stem height to water depth ratio	-
ϵ_b	Energy dissipation due to wave breaking	J m$^-$2 s$^-$1
ϵ_f	Energy dissipation due to bottom friction	J m$^-$2 s$^-$1
ϵ_v	Energy dissipation due to vegetation	J m$^-$2 s$^-$1
γ	Breaker index	-
ν	Kinematic viscosity of water	m^2/s
ω	Angular wave frequency	rad/s
ρ	Mass density of water	kg/m^3
σ_{max}	Flexural strength	MPa
σ_{wave}	Wave-induced bending stress	MPa
θ	Leaning angle	deg.
ζ	Water level	m+NAP
a, b, c	Fitting parameters in relation C_D and Re	-
A_c	Correction factor wave-induced stress	-
b_v	Stem diameter	m
$b_{v,in}$	Inner stem diameter	m
C_D	Bulk drag coefficient	-
C_F	Friction coefficient	-
c_g	Group velocity	m/s
E	Young's modulus	N/m^2
E	Wave energy density	J/m^2
f_{br}	Fraction of broken stems	-
F_{max}	Maximum force	N
g	Gravitational acceleration	m/s^2
h	Water depth	m
H	Wave height	m
$H_{1/10}$	Mean of highest 1/10th of waves	m
H_{m0}	Significant wave height	m
H_{rms}	Root mean square wave height	m
h_v	(Total) vegetation height	m
$h_{v,r}$	Reduced vegetation height after leaning	m
$h_{v,br}$	Stem height broken stems	m
I	Area moment of inertia	m^4
k	Wave number	rad/m
k_N	Nikuradse roughness length scale	m
L_{span}	Span length	m
M_{max}	Maximum moment	Nm
N_v	Stem density	stems/m^2
q_D	Wave-induced distributed load	N/m
Re	Vegetation Reynolds number	-
T	Wave period	s
T_p	Wave peak period	s
u	Amplitude of horizontal orbital velocity	m/s
u_{crit}	Critical orbital velocity for breakage	m/s
x	Distance along transect	m
y	Distance center to convex surface	m
z	Distance from water surface	m

Acknowledgements

This work is part of the research programme BE SAFE, which is financed by the Netherlands Organisation for Scientific Research (NWO). Additional financial support has been provided by Deltares, Boskalis, Van Oord, Rijkswaterstaat, World Wildlife Fund and HZ University of Applied Science. Bas W. Borsje was supported by the Netherlands Organization for Scientific Research (NWO-STW-VENI; 14363). We thank Franziska Rupprecht for providing the three-point-bending test data from the Hydralab experiments, for model validation.

References

Anderson, M. E. and McKee Smith, J. (2014). "Wave attenuation by flexible, idealized salt marsh vegetation." *Coastal Engineering*, 83, 82–92.

Anderson, M. E., McKee Smith, J., and McKay, S. K. (2011). *Wave dissipation by vegetation*. US Army Corps of Engineers (sep).

Arkema, K. K., Guannel, G., Verutes, G., Wood, S. A., Guerry, A., Ruckelshaus, M., Kareiva, P., Lacayo, M., and Silver, J. M. (2013). "Coastal habitats shield people and property from sea-level rise and storms." *Nature Climate Change*, 3(10), 913–918.

Barbier, E. B., Hacker, S. D., Kennedy, C., Koch, E. W., Stier, A. C., and Silliman, B. R. (2011). "The value of estuarine and coastal ecosystem services." *Ecological Monographs*, 81(2), 169–193.

Battjes, J. A. and Janssen, J. P. F. M. (1978). "Energy loss and set-up due to breaking of random waves." *Coastal Engineering Proceedings*, 32(1), 569–587.

Battjes, J. A. and Stive, M. J. F. (1985). "Calibration and verification of a dissipation model for random breaking waves." *Journal of Geophysical Research*, 90(C5), 649–660.

Booij, N., Ris, R. C. R., and Holthuijsen, L. H. L. (1999). "A third-generation wave model for coastal regions. I- Model description and validation." *Journal of geophysical research*, 104(C4), 7649–7666.

Bouma, T. J., de Vries, M. B., and Herman, P. M. J. (2010). "Comparing ecosystem engineering efficiency of two plant species with contrasting growth strategies.." *Ecology*, 91(9), 2696–2704.

873 Bouma, T. J., De Vries, M. B., Low, E., Peralta, G., Tánczos, I. C., van de Koppel, J., and
874 Herman, P. M. J. (2005). "Trade-Offs Related To Ecosystem Engineering: a Case Study on
875 Stiffness of Emerging Macrophytes." *Ecology*, 86(8), 2187–2199.

876 Bouma, T. J., van Belzen, J., Balke, T., Zhu, Z., Airoldi, L., Blight, A. J., Davies, A. J., Galvan,
877 C., Hawkins, S. J., Hoggart, S. P. G., Lara, J. L., Losada, I. J., Maza, M., Ondiviela, B., Skov,
878 M. W., Strain, E. M., Thompson, R. C., Yang, S., Zanuttigh, B., Zhang, L., and Herman,
879 P. M. J. (2014). "Identifying knowledge gaps hampering application of intertidal habitats in
880 coastal protection: Opportunities & steps to take." *Coastal Engineering*, 87, 147–157.

881 Dalrymple, R. A., Kirby, J. T., and Hwang, P. A. (1984). "Wave diffraction due to areas of energy
882 dissipation." *Journal of Waterway, Port, Coastal and Ocean Engineering*, 110(1), 67–79.

883 de Langre, E. (2012). "Methodological advances in predicting flow-induced dynamics of plants
884 using mechanical-engineering theory." *Journal of Experimental Biology*, 215, 914–921.

885 Dijkstra, J. T. and Uittenbogaard, R. E. (2010). "Modeling the interaction between flow and
886 highly flexible aquatic vegetation." *Water Resources Research*, 46(12), 1–14.

887 Drake, B. G. (1976). "Seasonal changes in reflectance and standing crop biomass in three salt
888 marsh communities.." *Plant physiology*, 58(5), 696–9.

889 Duarte, C. M., Losada, I. J., Hendriks, I. E., Mazarrasa, I., and Marba, N. (2013). "The role
890 of coastal plant communities for climate change mitigation and adaptation." *Nature Clim.*
891 *Change*, 3(11), 961–968.

892 Feagin, R. A., Irish, J. L., Möller, I., Williams, A. M., Colón-Rivera, R. J., and Mousavi, M. E.
893 (2011). "Short communication: Engineering properties of wetland plants with application to
894 wave attenuation." *Coastal Engineering*, 58(3), 251–255.

895 Gallagher, J. L. (1983). "Seasonal patterns in recoverable underground reserves in Spartina
896 alterniflora Loisel (Delaware, Georgia).." *American Journal of Botany*, 70(2), 212–215.

897 Gere, J. M. and Goodno, B. J. (2013). *Mechanics of Materials*. Cengage Learning, Stamford,
898 USA, 8th edition.

899 Grüne, J. (2005). "Evaluation of wave climate parameters from benchmarking flotsam levels."
900 *Proceedings of the International Conference on Coastlines, Structures and Breakwaters, 2005*,
901 Thomas Telford, 468.

902 Harley, C. D. G. and Bertness, M. D. (1996). "Structural interdependence: An ecological con-
903 sequence of morphological responses to crowding in marsh plants." *Functional Ecology*, 10(5),
904 654–661.

905 Heuner, M., Silinski, A., Schoelynck, J., Bouma, T. J., Puijalon, S., Troch, P., Fuchs, E.,
906 Schröder, B., Schröder, U., Meire, P., and Temmerman, S. (2015). "Ecosystem engineer-
907 ing by plants on wave-exposed intertidal flats is governed by relationships between effect and
908 response traits." *PLoS ONE*, 10(9), 1–18.

909 Howes, N. C., FitzGerald, D. M., Hughes, Z. J., Georgiou, I. Y., Kulp, M. A., Miner, M. D.,
910 Smith, J. M., and Barras, J. A. (2010). "Hurricane-induced failure of low salinity wetlands."
911 *Proceedings of the National Academy of Sciences of the United States of America*, 107(32),
912 14014–14019.

913 Hu, Z., Suzuki, T., Zitman, T. J., Uittewaal, W., Stive, M. J. F., Uijttewaal, W. S. J., and
914 Stive, M. J. F. (2014). "Laboratory study on wave dissipation by vegetation in combined
915 current-wave flow." *Coastal Engineering*, 88, 131–142.

916 Jadhav, R. S., Chen, Q., and McKee Smith, J. (2013). "Spectral distribution of wave energy
917 dissipation by salt marsh vegetation." *Coastal Engineering*, 77, 99–107.

918 Kobayashi, N., Raichle, A. W., and Asano, T. (1993). "Wave Attenuation by Vegetation."
919 *Journal of Waterway, Port, Coastal, and Ocean Engineering*, 119(1), 30–48.

920 Koch, E. W., Barbier, E. B., Silliman, B. R., Reed, D. J., Perillo, G. M., Hacker, S. D., Granek,
921 E. F., Primavera, J. H., Muthiga, N., Polasky, S., Halpern, B. S., Kennedy, C. J., Kappel,
922 C. V., and Wolanski, E. (2009). "Non-linearity in ecosystem services: Temporal and spatial
923 variability in coastal protection." *Frontiers in Ecology and the Environment*, 7(1), 29–37.

924 Liffen, T., Gurnell, M. A., O'Hare, M. T., Pollen-Bankhead, N., Simon, A., Gurnell, A. M.,
925 O'Hare, M. T., Pollen-Bankhead, N., and Simon, A. (2013). "Associations between the mor-
926 phology and biomechanical properties of Sparganium erectum: Implications for survival and
927 ecosystem engineering." *Aquatic Botany*, 105, 18–24.

928 Luhar, M., Coutu, S., Infantes, E., Fox, S., and Nepf, H. M. (2010). "Wave-induced velocities
929 inside a model seagrass bed." *Journal of Geophysical Research: Oceans*, 115(12), 1–15.

930 Luhar, M. and Nepf, H. M. (2011). "Flow-induced reconfiguration of buoyant and flexible aquatic
931 vegetation." *Limnology and Oceanography*, 56(6), 2003–2017.

Luhar, M. and Nepf, H. M. (2016). "Wave-induced dynamics of flexible blades." *Journal of Fluids and Structures*, 61, 20–41.

Mach, K. J., Hale, B. B., Denny, M. W., and Nelson, D. V. (2007). "Death by small forces: a fracture and fatigue analysis of wave-swept macroalgae.." *The Journal of experimental biology*, 210(Pt 13), 2231–2243.

Madsen, O. S., Poon, Y.-K., and Graber, H. C. (1988). "Spectral Wave Attenuation by Bottom Friction: Theory." *Proceedings of the 21th Int. Conf. Coastal Engineering*, 492–504.

Marsooli, R. and Wu, W. (2014). "Numerical investigation of wave attenuation by vegetation using a 3D RANS model." *Advances in Water Resources*, 74(October), 245–257.

Mendez, F. J. and Losada, I. J. (2004). "An empirical model to estimate the propagation of random breaking and nonbreaking waves over vegetation fields." *Coastal Engineering*, 51(2), 103–118.

Méndez, F. J. F., Losada, I. J., and Losada, M. A. (1999). "Hydrodynamics induced by wind waves in a vegetation field." *Journal of Geophysical Research*, 104(C8), 18383.

Miler, O., Albayrak, I., Nikora, V., and O'Hare, M. (2012). "Biomechanical properties of aquatic plants and their effects on plant-flow interactions in streams and rivers." *Aquatic Sciences*, 74(1), 31–44.

Möller, I., Kudella, M., Rupprecht, F., Spencer, T., Paul, M., van Wesenbeeck, B. K., Wolters, G., Jensen, K., Bouma, T. J., Miranda-Lange, M., and Schimmels, S. (2014). "Wave attenuation over coastal salt marshes under storm surge conditions." *Nature Geoscience*, 7(10), 727–731.

Mullarney, J. C. and Henderson, S. M. (2010). "Wave-forced motion of submerged single-stem vegetation." *Journal of Geophysical Research*, 115(C12), C12061.

Nelson, R. C. (1994). "Depth limited design wave heights in very flat regions." *Coastal Engineering*, 23(1), 43–59.

O'Donnell, J. P. R. and Schalles, J. F. (2016). "Examination of abiotic drivers and their influence on Spartina alterniflora biomass over a twenty-eight year period using Landsat 5 TM satellite imagery of the Central Georgia Coast." *Remote Sensing*, 8(6).

Paquier, A. E., Haddad, J., Lawler, S., and Ferreira, C. M. (2016). "Quantification of the Attenuation of Storm Surge Components by a Coastal Wetland of the US Mid Atlantic." *Estuaries and Coasts*, 1–17.

Paul, M. and Amos, C. L. (2011). "Spatial and seasonal variation in wave attenuation over Zostera noltii." *Journal of Geophysical Research: Oceans*, 116(C08019), 1–16.

Paul, M., Henry, P. Y. T., and Thomas, R. E. (2014). "Geometrical and mechanical properties of four species of northern European brown macroalgae." *Coastal Engineering*, 84, 73–80.

Paul, M., Rupprecht, F., Möller, I., Bouma, T. J., Spencer, T., Kudella, M., Wolters, G., van Wesenbeeck, B. K., Jensen, K., Miranda-Lange, M., and Schimmels, S. (2016). "Plant stiffness and biomass as drivers for drag forces under extreme wave loading: A flume study on mimics." *Coastal Engineering*, 117, 70–78.

Puijalon, S., Bouma, T. J., Douady, C. J., van Groenendael, J., Anten, N. P. R., Martel, E., and Bornette, G. (2011). "Plant resistance to mechanical stress: Evidence of an avoidance-tolerance trade-off." *New Phytologist*, 191(4), 1141–1149.

Rupprecht, F., Möller, I., Evans, B., Spencer, T., Jensen, K., M??ller, I., Evans, B., Spencer, T., and Jensen, K. (2015). "Biophysical properties of salt marsh canopies - Quantifying plant stem flexibility and above ground biomass." *Coastal Engineering*, 100, 48–57.

Rupprecht, F., Möller, I., Paul, M., Kudella, M., Spencer, T., van Wesenbeeck, B. K., Wolters, G., Jensen, K., Bouma, T. J., Miranda-Lange, M., and Schimmels, S. (2017). "Vegetation-wave interactions in salt marshes under storm surge conditions." *Ecological Engineering*, 100, 301–315.

Schroevers, M., Huisman, B. J. A., Van Der Wal, M., and Terwindt, J. (2011). "Measuring ship induced waves and currents on a tidal flat in the Western Scheldt Estuary." *2011 IEEE/OES/CWTM 10th Working Conference on Current, Waves and Turbulence Measurement, CWTM 2011*, 123–129.

Seymour, R. J., Tegner, M. J., and Seymour M.J. Tegner, P.K. Dayton, & P.E. Parnell., R. J. (1989). "Storm wave induced mortality of Giant Kelp, Macrocystis pyrifera, in southern California.." *Est., Coastal & Shelf Sci.*, 28(3), 277–292.

Silinski, A., Heuner, M., Schoelynck, J., Puijalon, S., Schröder, U., Fuchs, E., Troch, P., Bouma, T. J., Meire, P., and Temmerman, S. (2015). "Effects of wind waves versus ship waves on tidal

marsh plants: A flume study on different life stages of scirpus maritimus." *PLoS ONE*, 10(3), 1–16.

Suzuki, T., Zijlema, M., Burger, B., Meijer, M. C., and Narayan, S. (2012). "Wave dissipation by vegetation with layer schematization in SWAN." *Coastal Engineering*, 59(1), 64–71.

Tang, J., Shen, S., and Wang, H. (2015). "Numerical model for coastal wave propagation through mild slope zone in the presence of rigid vegetation." *Coastal Engineering*, 97(March), 53–59.

Temmerman, S., Meire, P., Bouma, T. J., Herman, P. M. J., Ysebaert, T., and De Vriend, H. J. (2013). "Ecosystem-based coastal defence in the face of global change." *Nature*, 504(7478), 79–83.

Tschirky, P., Hall, K., and Turcke, D. (2001). "Wave attenuation by emergent wetland vegetation." *Coastal Engineering*, 865–877.

Usherwood, J. R., Ennos, A. R., and Ball, D. J. (1997). "Mechanical and anatomical adaptations in terrestrial and aquatic buttercups to their respective environments." *Journal of Experimental Botany*, 48(312), 1469–1475.

Vuik, V., Jonkman, S. N., Borsje, B. W., and Suzuki, T. (2016). "Nature-based flood protection: The efficiency of vegetated foreshores for reducing wave loads on coastal dikes." *Coastal Engineering*, 116, 42–56.

Weitzman, J. S., Zeller, R. B., Thomas, F. I. M., and Koseff, J. R. (2015). "The attenuation of current- and wave-driven flow within submerged multispecific vegetative canopies." *Limnology and Oceanography*, 60(6), 1855–1874.

Highlights

- Wave attenuation by vegetation and vegetation characteristics exhibit a seasonal variation
- A model has been developed for prediction of vegetation stem breakage by waves
- The model reasonably reproduces measured stem breakage in a large wave flume
- There are clear differences in stability between two contrasting plant species